NASA
Technical
Paper
2702

April 1987

# Experimental Evaluation of Blockage Ratio and Plenum Evacuation System Flow Effects on Pressure Distribution for Bodies of Revolution in 0.1-Scale Model Test Section of NASA Lewis Research Center's Proposed Altitude Wind Tunnel

Richard R. Burley and
Douglas E. Harrington

NASA

**NASA Technical Paper 2702**

1987

# Experimental Evaluation of Blockage Ratio and Plenum Evacuation System Flow Effects on Pressure Distribution for Bodies of Revolution in 0.1-Scale Model Test Section of NASA Lewis Research Center's Proposed Altitude Wind Tunnel

Richard R. Burley and
Douglas E. Harrington

*Lewis Research Center*
*Cleveland, Ohio*

National Aeronautics
and Space Administration

**Scientific and Technical
Information Branch**

## Summary

An experimental investigation was conducted in the slotted test section of the 0.1-scale model of the proposed Altitude Wind Tunnel. The slotted test section, which had an 11-percent open area ratio, was surrounded by a plenum chamber. The objective was to evaluate wall interference effects at tunnel Mach numbers from 0.70 to 0.95 on bodies of revolution with blockage ratios of 0.43, 3, 6, and 12 percent. The amount of flow that had to be removed from the plenum tank by the plenum evacuation system (PES) to eliminate wall interference effects was determined. The effectiveness of the tunnel reentry flaps in removing flow from the plenum tank was examined with the 3-percent model installed.

Results showed that the 0.43-percent blockage model was the only one free of wall interference effects with no PES flow. Surface pressures on the forward part of the 3-, 6-, and 12-percent blockage models were greater than interference-free results and were not influenced by PES flow. Interference-free results were achieved on the aft part of the 3- and 6-percent blockage models with the proper amount of PES flow but not on the aft part of the 12-percent blockage model because so much of this model extended downstream of the test section. The use of tunnel reentry flaps was very effective in reducing the amount of PES flow required.


## Introduction

It has been proposed that the NASA Lewis Research Center rehabilitate and extend the capabilities of its Altitude Wind Tunnel (AWT) to meet the aeropropulsion needs of the next century. The AWT (fig. 1) was first brought on line in 1944 and was used for aeropropulsion research until 1958, when it was converted into a series of altitude test chambers for space research. As originally configured, the AWT had a maximum Mach number of 0.6 at an altitude of 9140 m (30 000 ft) with static temperature capability down to −54 °C (−65 °F). Because all the internal components were removed in the conversion, the proposed AWT would require all new internal components.

The planned rehabilitated tunnel (fig. 2) would have an expanded Mach number capability of 0.9+, altitude pressures up to 16 800 m (55 000 ft), and total temperature capability down to −51 °C (−60 °F). New capabilities would include adverse weather test environments (icing, freezing rain, heavy rain, and snow) and acoustical instrumentation in the test section. The proposed rehabilitated AWT is described more completely in references 1 to 4.

Because of the magnitude of the AWT rehabilitation and the significant extensions to its original capability, a modeling program (both experimental and analytical) comprising several 0.1-scale models was undertaken to ensure the technical soundness of the new component designs. The 0.1-scale model size was selected because of facility modeling experience at this scale (refs. 5 and 6) and because it represented the upper limit of the exhaust flow capability available at NASA Lewis for providing model airflow. Experimental results concerning some components of the modeling program are reported in references 7 to 12.

One of the 0.1-scale models was the high-speed leg, which included a slotted test section surrounded by a plenum chamber. An experimental investigation was conducted in this 0.1-scale model to evaluate wall interference effects in the high subsonic speed range on bodies of revolution. The amount of flow that had to be removed from the plenum chamber by a plenum evacuation system (PES) to eliminate wall interference effects was determined. The effectiveness of tunnel reentry flaps in removing flow from the plenum chamber was examined with the 3-percent model installed. The results are presented in this report.

The bodies of revolution had blockage ratios of 0.43, 3, 6, and 12 percent. They were tested over a range of Mach numbers from 0.70 to 0.95 and at PES flows from 0 to 10 percent of the tunnel flow.

The interference effect was evaluated by comparing the pressure coefficient distribution obtained on the body-of-revolution surface in the 0.1-scale model test section with data obtained on a geometrically similar body of revolution in NASA Langley Research Center's 16-Foot Transonic Wind Tunnel. The NASA Langley data were considered to be free of wall interference over the Mach number range of interest.

## Symbols

$C_p$ pressure coefficient

$L$ length, cm (in.)

$L_R$ model reference length (not a physical length but a constant that is necessary to achieve the proper shape of each model (ref. 13))

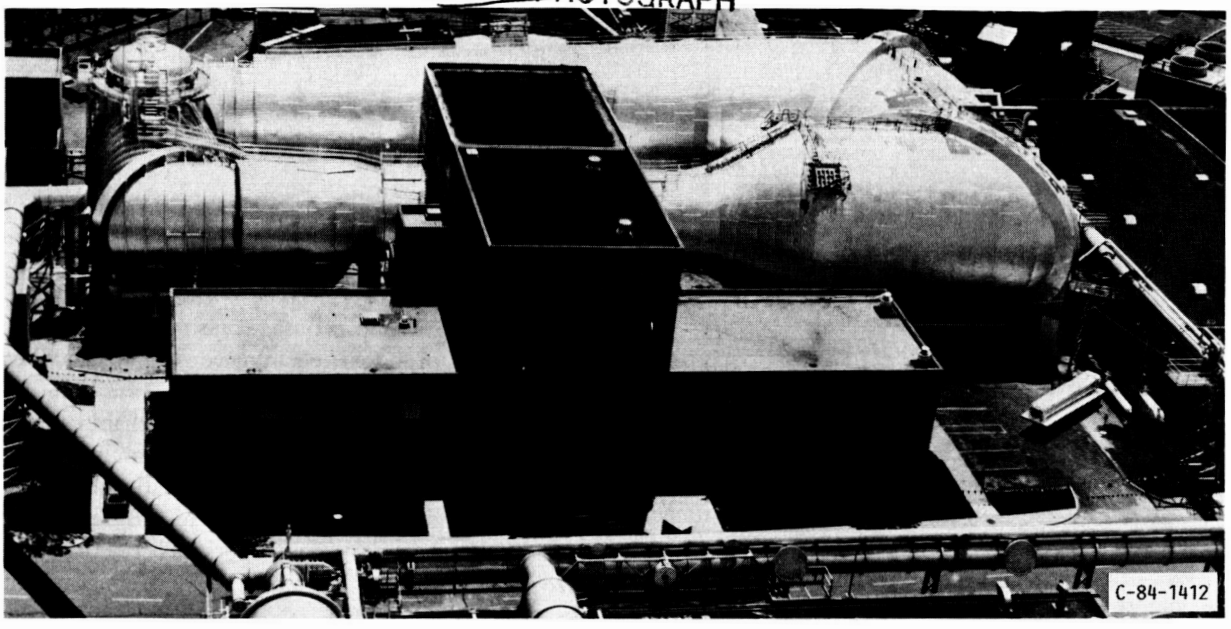


Figure 1.—Configuration of Lewis Research Center's Altitude Wind Tunnel.

$M$ Mach number
$P$ total pressure, $N/m^2$ (psi)
$p$ static pressure, $N/m^2$ (psi)
$R$ model radius, cm (in.)
$x$ axial distance, cm (in.)
$Z$ radius associated with total pressure rakes, cm (in.)
$\theta$ circumferential location of static taps on tunnel walls, deg
$\varphi$ circumferential location of static taps on models, deg
$\psi$ circumferential location of total pressure rakes, deg

Subscripts:

$cs$ contraction-section entrance
$pl$ plenum chamber
$ts$ test section
$w$ test-section wall

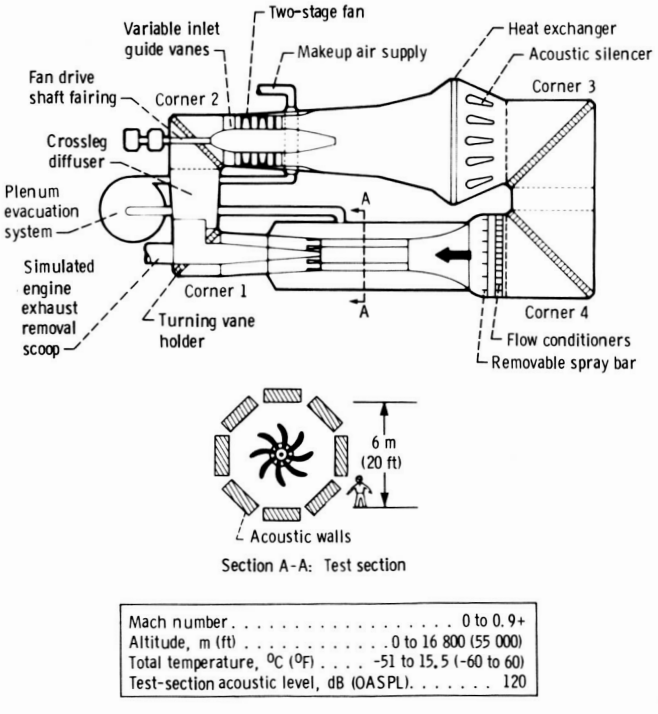


| | |
|---|---|
| Mach number | 0 to 0.9+ |
| Altitude, m (ft) | 0 to 16 800 (55 000) |
| Total temperature, °C (°F) | -51 to 15.5 (-60 to 60) |
| Test-section acoustic level, dB (OASPL) | 120 |

Figure 2.—Capabilities of modified and rehabilitated AWT.

## Apparatus and Procedure

### Test Apparatus

The investigation was conducted in the 0.1-scale model of the high-speed leg proposed for the Lewis Research Center's Altitude Wind Tunnel (figs. 3 and 4). It models the settling chamber and the contraction, test, and diffuser sections.

The octagonal test section (fig. 5) was 167.6 cm (66 in.) long with eight longitudinal slots at the vertices of the octagon. The slots, which were closed at the entrance to the test section, opened linearly to their full width at 30.5 cm (12 in.) into the test section. The width remained constant for 134.6 cm (53 in.) and then opened linearly again for the final 2.5 cm (1 in.) of the test section. The top, bottom, and side walls did not diverge. The other four walls diverged to account for boundary-layer growth. The nominal test-section open area at any axial location downstream of 30.5 cm (12 in.) into the

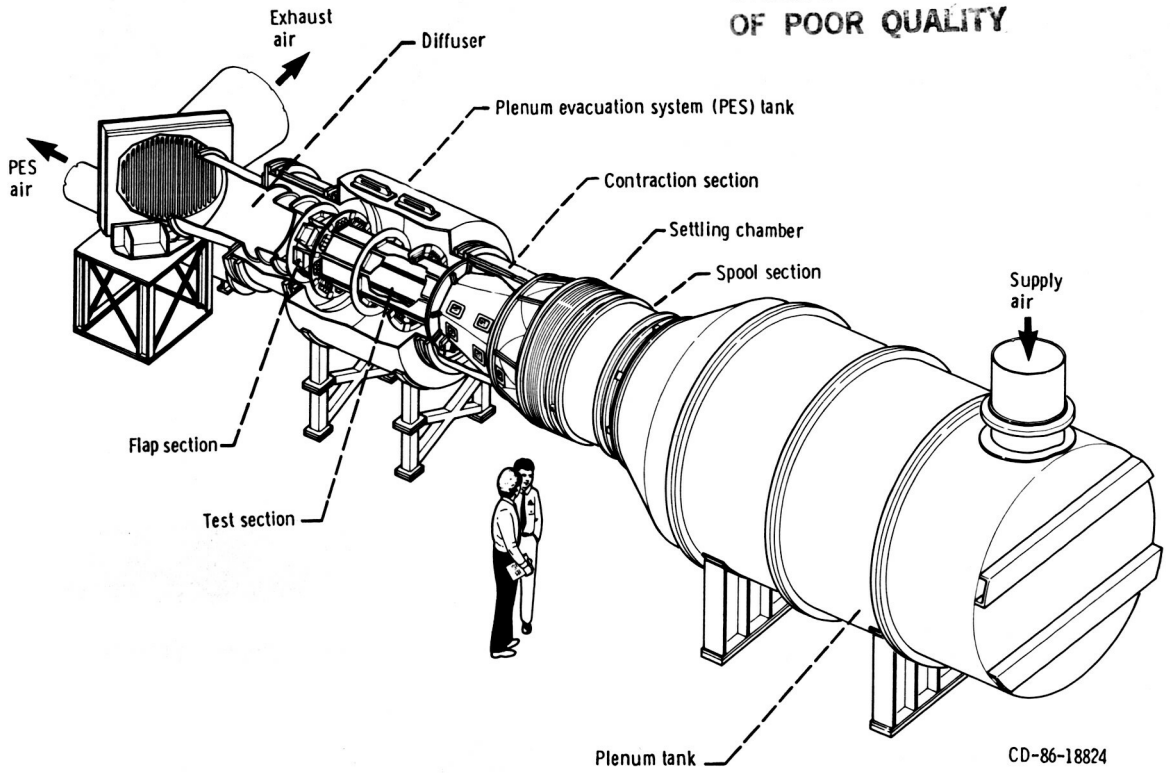


Figure 3.—Schematic of test facility.

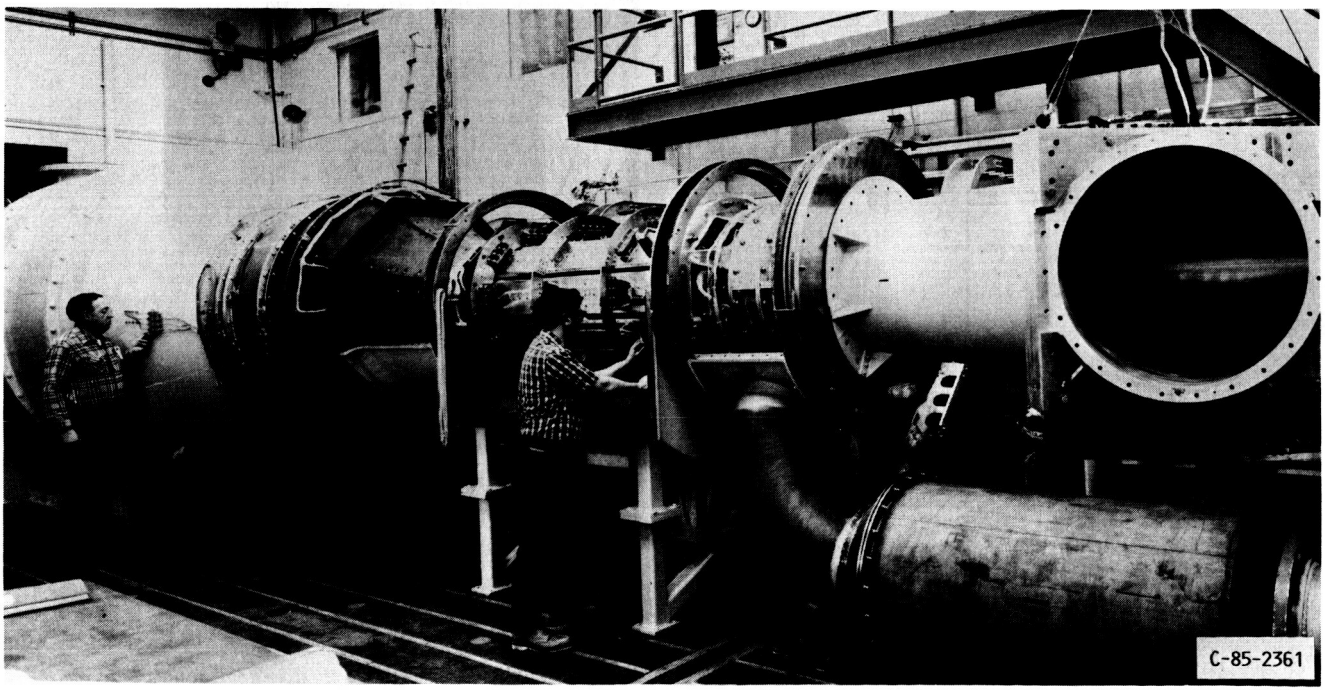


Figure 4.—Test facility (as seen from other side).

test section was 11 percent based on the perimeter of a closed octagon. More detailed information concerning the test section is given in reference 11.

The test section, along with parts of the contraction section and diffuser, was enclosed in a large plenum chamber (figs. 3 and 4). The plenum chamber was tied into the plenum evacuation system (PES) to provide boundary-layer and model blockage control in the test section. PES flow was exhausted

through a 45.7-m (18-in.) diameter pipe to the NASA Lewis altitude exhaust system. The exhaust pipe was attached to the aft part of the PES tank downstream of the test section (figs. 3 and 4). The plenum chamber for the 0.1-scale model should have been 121.9 cm (48 in.) in diameter. However, to provide adequate working space for installing instrumentation, the chamber was 182.9 cm (72 in.) in diameter. To maintain the proper scale during testing, a foam filler was used to reduce the chamber diameter to its proper value.

Adjacent to the downstream end of the test section was the flap section (fig. 6). A flap was located at the end of each test-section slot; each flap could be positioned from fully closed (0° with respect to the diffuser wall) to an angle of 9°. Most of the investigation was done with the flaps at 9° (figs. 6 and 7), but a part of the investigation was done with the flaps at 0° (figs. 6 and 8). Even at 0°, however, the flaps might pump some flow from the plenum chamber because of the shape of their upstream ends. To eliminate this pumping, inserts were installed over the upstream ends of the flaps (fig. 9). When positioned at any angle greater than 0°, the flaps pumped flow from the plenum tank into the diffuser to provide boundary-layer and model blockage control in the test section. Thus the flaps served the same purpose as the PES. However, the PES would require power for its operation, whereas the flaps would not.

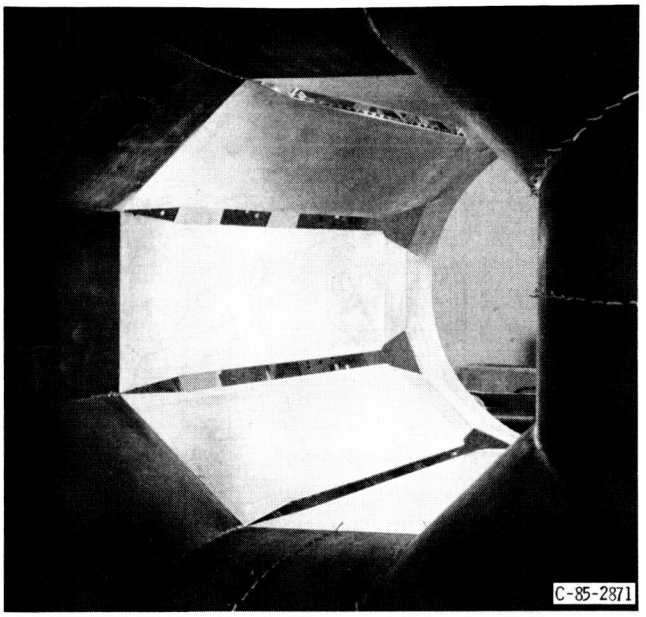


Figure 5.—Octagonal slotted test section (looking downstream).

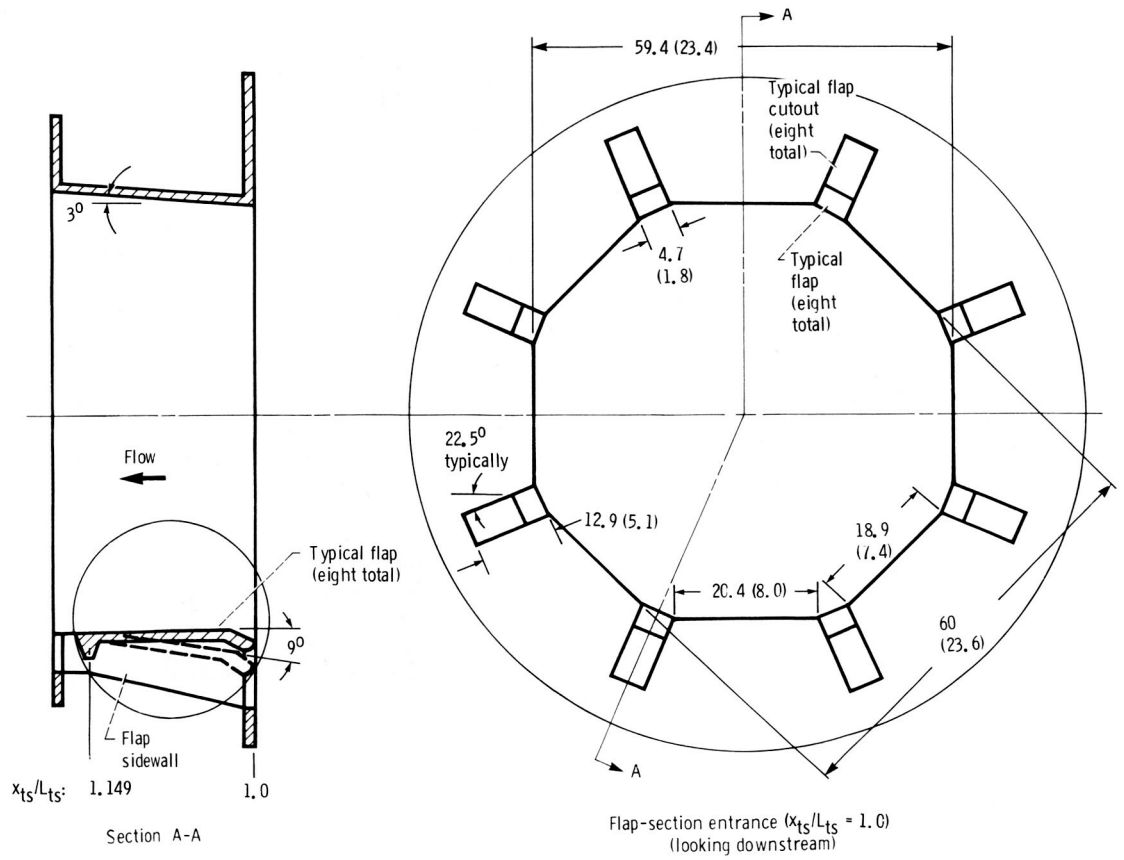


Figure 6.—Geometric details of flap section. (Linear dimensions are in centimeters (inches).)

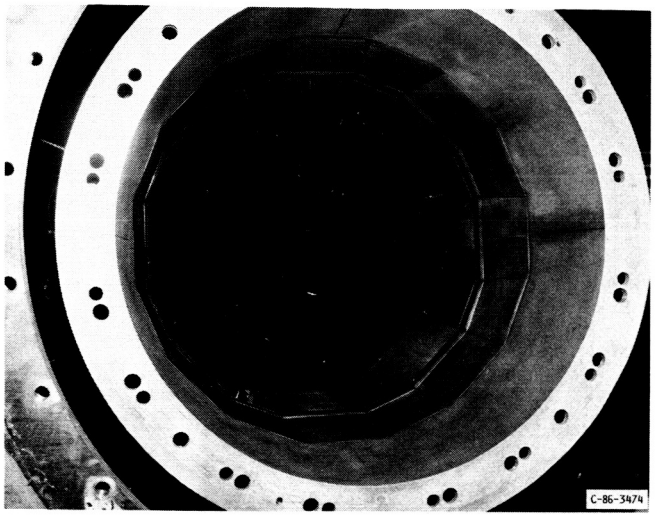


Figure 7.—Reentry flaps and octagonal slotted test section (looking upstream). Reentry flaps at 9°.

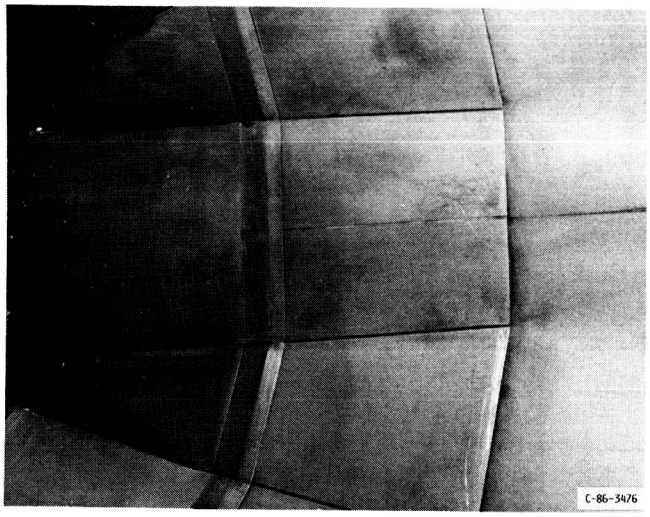


Figure 8.—Reentry flaps at 0° (looking upstream).

## Blockage Models

Originally the nose of each body of revolution, or blockage model, was to be located at an $x_{ts}/L_{ts}$ of 0.18 because the velocity profile there should be flat according to analytical results in reference 4. However, experimental results in reference 11 indicated a modest flow acceleration starting near the test-section entrance and ending midway into the test section ($x_{ts}/L_{ts} = 0.50$) over the tunnel Mach number range of interest for the present test (0.70 to 0.95). The rate of acceleration increased with increasing tunnel Mach number but was independent of flap angle and PES flow. Consequently $x_{ts}/L_{ts} = 0.50$ was selected as the preferred location for the nose of each model (fig. 10).

The model shape (fig. 10) was a blunt-nose, supercritical body of type C in reference 13. This model shape, as already mentioned, was tested in Langley's 16-Foot Transonic Wind Tunnel. The model shape, along with the model pressure coefficient distribution at tunnel Mach numbers of 0.70 to 0.95, is described completely in reference 13. Four blockage

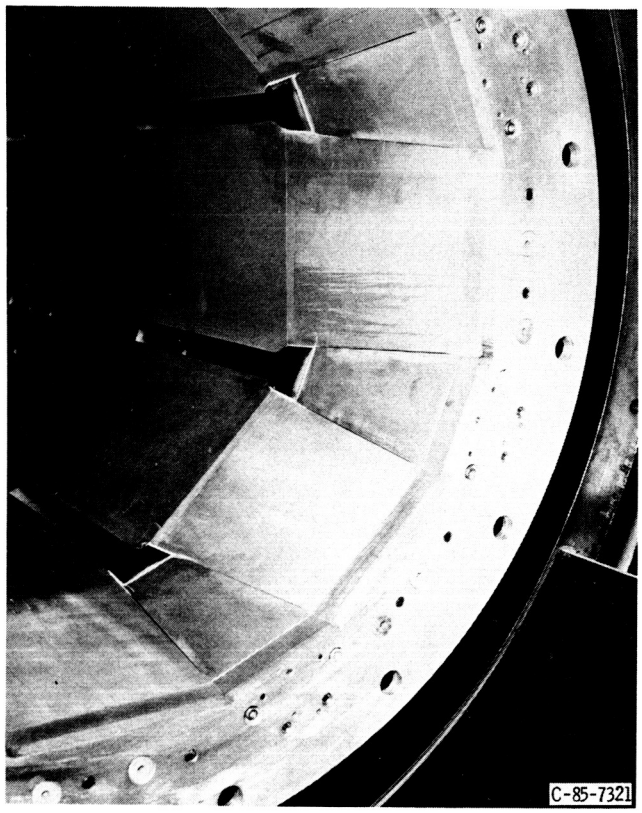


Figure 9.—Inserts over reentry flaps at 0° (looking upstream).

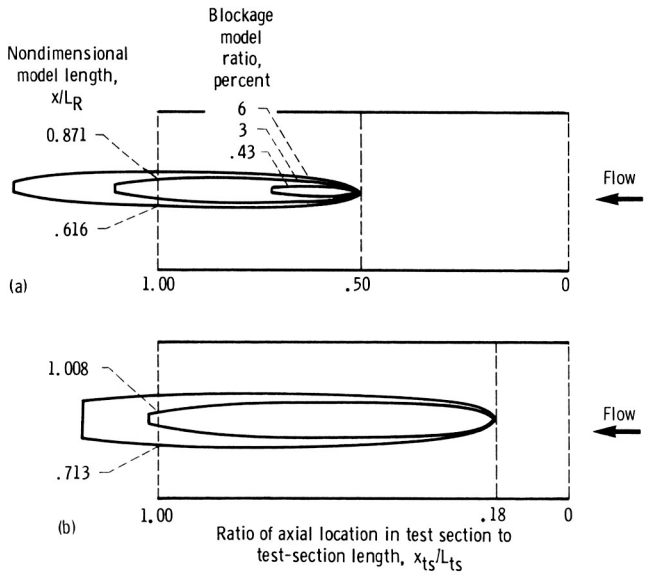


(a) 0.43-, 3-, and 6-Percent models.
(b) 12-Percent model.

Figure 10.—Axial location of blockage models in test section.

TABLE I.—MODELS AND STING DIMENSIONS

| Blockage, percent | Maximum diameter | | Model length, $L$ | | Reference model length, $L_R$ | | Base diameter | | Sting diameter | | Cylindrical sting length | | Included angle of sting flare, deg |
|---|---|---|---|---|---|---|---|---|---|---|---|---|---|
| | cm | in. | cm | in. | cm | in. | cm | in. | cm | in. | cm | in. | |
| 0.43 | 4.01 | 1.58 | 38.38 | 15.11 | 36.45 | 14.35 | 0.97 | 0.38 | 0.89 | 0.35 | 6.55 | 2.58 | 6 |
| 3.00 | 10.59 | 4.17 | 101.37 | 39.91 | 96.24 | 37.89 | 2.74 | 1.08 | 2.34 | .92 | 17.30 | 6.81 | 6 |
| 6.00 | 14.99 | 5.90 | 143.36 | 56.44 | 136.12 | 53.59 | 3.89 | 1.53 | 3.30 | 1.30 | 24.46 | 9.63 | 6 |
| 12.00 | 21.18 | 8.34 | 202.72 | 79.81 | 192.48 | 75.78 | 5.49 | 2.16 | 4.67 | 1.84 | 34.57 | 13.61 | 0 |

ratio models were investigated in the present test: 0.43, 3, 6, and 12 percent. The noses of three models (0.43, 3, and 6 percent) were located midway into the test section (at $x_{ts}/L_{ts} = 0.50$). Since a large extent of the 6-percent blockage model was downstream of the test-section exit, this model was also located at $x_{ts}/L_{ts} = 0.18$. The nose of the 12-percent blockage model was located only at $x_{ts}/L_{ts} = 0.18$. This model was too long for its nose to be located at $x_{ts}/L_{ts} = 0.50$. The centerline of each model coincided with the test-section centerline. All models were constructed of stainless steel with a radial tolerance of $\pm 0.0025$ cm ($\pm 0.0010$ in.) and a surface finish of 32. Pertinent dimensions of all models and stings are listed in table I, and model coordinates are given in table II.

TABLE II.—NONDIMENSIONAL MODEL COORDINATES

| $x/L_R$ | $R/L_R$ | $x/L_R$ | $R/L_R$ |
|---|---|---|---|
| 0 | 0 | 0.4000 | 0.05443 |
| .0020 | .00713 | .4500 | ----- |
| .0040 | .00969 | .4800 | .05500 |
| .0050 | ----- | .5000 | .05495 |
| .0060 | .01159 | .5500 | ----- |
| .0075 | ----- | .6000 | .05358 |
| .0080 | .01316 | .6500 | ----- |
| .0100 | .01450 | .6800 | .05107 |
| .0120 | .01570 | .7000 | ----- |
| .0125 | ----- | .7200 | .04934 |
| .0140 | .01678 | .7500 | ----- |
| .0160 | .01777 | .7600 | .04725 |
| .0180 | .01868 | .8000 | .04481 |
| .0200 | .01954 | .8200 | .04344 |
| .0250 | ----- | .8400 | .04196 |
| .0400 | .02604 | .8500 | ----- |
| .0500 | ----- | .8600 | .04037 |
| .0600 | .03060 | .8800 | .03867 |
| .0750 | ----- | .9000 | .03683 |
| .0800 | .03416 | .9030 | ----- |
| .1000 | .03709 | .9200 | .03484 |
| .1200 | .03958 | .9400 | .03268 |
| .1400 | .04172 | .9600 | .03032 |
| .1500 | ----- | .9700 | .02906 |
| .1600 | .04360 | .9800 | .02773 |
| .1800 | .04525 | .9900 | .02632 |
| .2000 | .04671 | 1.0000 | .02483 |
| .2400 | .04915 | 1.0100 | .02323 |
| .2500 | ----- | 1.0200 | .02150 |
| .2800 | .05108 | 1.0300 | .01962 |
| .3000 | ----- | 1.0400 | .01753 |
| .3200 | .05256 | 1.0450 | .01642 |
| .3500 | ----- | 1.0532 | .01423 |

All blockage models (fig. 10), except the 0.43-percent blockage model, were too long to be contained within the test section. The nondimensional model lengths at the test-section exit $x/L_R$ were 0.871 and 0.616 for the 3- and 6-percent blockage models, respectively, with their noses at $x_{ts}/L_{ts} = 0.50$, and 1.008 and 0.713 for the 6- and 12-percent blockage models, respectively, with their noses at $x_{ts}/L_{ts} = 0.18$. The 3-percent blockage model installed in the slotted test section is shown in figure 11.

## Stings

In all tests the blockage models were supported by stings. Each sting extended into the diffuser and was mounted to a strut (fig. 12). The stings were designed in accordance with reference 14 to minimize their interference on the flow over the aft end of the blockage models. They were geometrically similar to the stings used in reference 13. All stings, except the one for the 12-percent blockage model, flared out at an included angle of about 6° to a maximum diameter of 4.7 cm (1.8 in.). This diameter is greater than the maximum diameter of the 0.43-percent blockage model. The sting for the 12-percent blockage model had a constant diameter of 4.7 cm (1.8 in.). Pertinent sting dimensions are presented in table I.

## Instrumentation

Tunnel and PES mass flow rates were measured with standard ASME sharp-edge orifice plates. Orifice temperatures were measured with copper-constantan thermocouples, and orifice pressures with individual transducers.

Both the blockage models and the test-section walls were instrumented. Each blockage model had 42 static pressure taps (table III), 24 of which were at a circumferential location of 0°. Each of the eight test-section flats had 27 static pressure taps equally spaced 6.4 cm (2.5 in.) apart on the centerline (fig. 13). All static taps were 0.051 cm (0.020 in.) in diameter and were installed flush and perpendicular to the surface.

Additional instrumentation—total pressure rakes at the contraction-section entrance (fig. 14) and static pressure taps

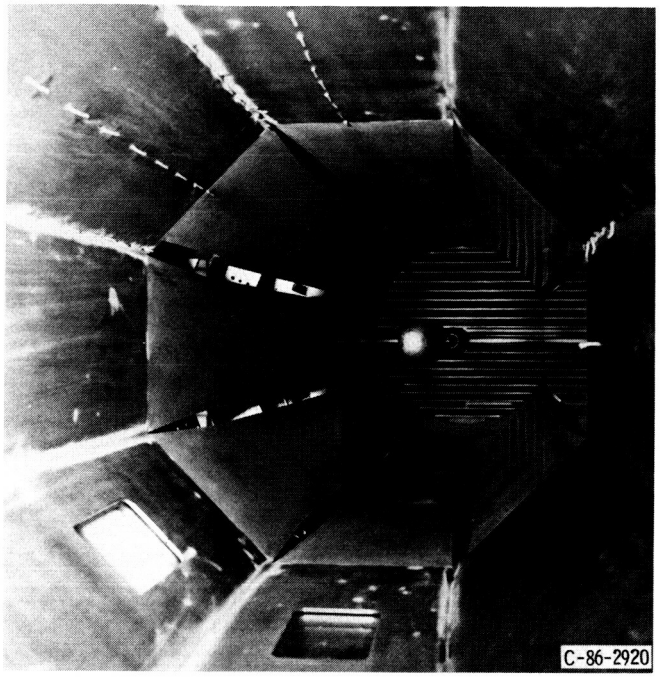


Figure 11.—3-Percent blockage model installed in octagonal slotted test section.

in the plenum chamber—was required to set the tunnel Mach number. (The method of setting the tunnel Mach number is described in the appendix.)

TABLE III.—NONDIMENSIONAL PRESSURE ORIFICE LOCATIONS ON BLOCKAGE MODELS

| Axial location, $x/L_R$ | Circumferential location, $\varphi$, deg | Axial location, $x/L_R$ | Circumferential location, $\varphi$, deg |
|---|---|---|---|
| 0 | 0 | 0.783 | 0, 90, 180 |
| .045 | 0, 90, 180, 270 | .854 | 0 |
| .107 | 0 | .872 | 0 |
| .142 | 0, 90, 180, 270 | .890 | 0, 90, 180 |
| .214 | 0 | .908 | 0 |
| .285 | 0 | .926 | 0 |
| .356 | 0, 90, 180 | .943 | 0, 90, 180 |
| .427 | 0 | .961 | 0 |
| .498 | 0 | .979 | 0 |
| .570 | 0, 90, 180 | .997 | 0 |
| .641 | 0 | 1.015 | 0, 90, 180 |
| .712 | 0 | 1.032 | 0 |

All pressures except orifice pressures were measured with an electronically scanned pressure system. The system consisted of a number of modules, each of which contained 32 individual transducers. Static pressures on the blockage models were measured with $\pm 103.4$-kN/m$^2$ ($\pm 15$-psid) transducers having an accuracy of $\pm 0.14$ N/m$^2$ ($\pm 0.02$ psi). Test-section wall static pressures were measured with $\pm 34.5$-kN/m$^2$ ($\pm 5$-psid) transducers having an accuracy of $\pm 0.048$ kN/m$^2$ ($\pm 0.007$ psi).

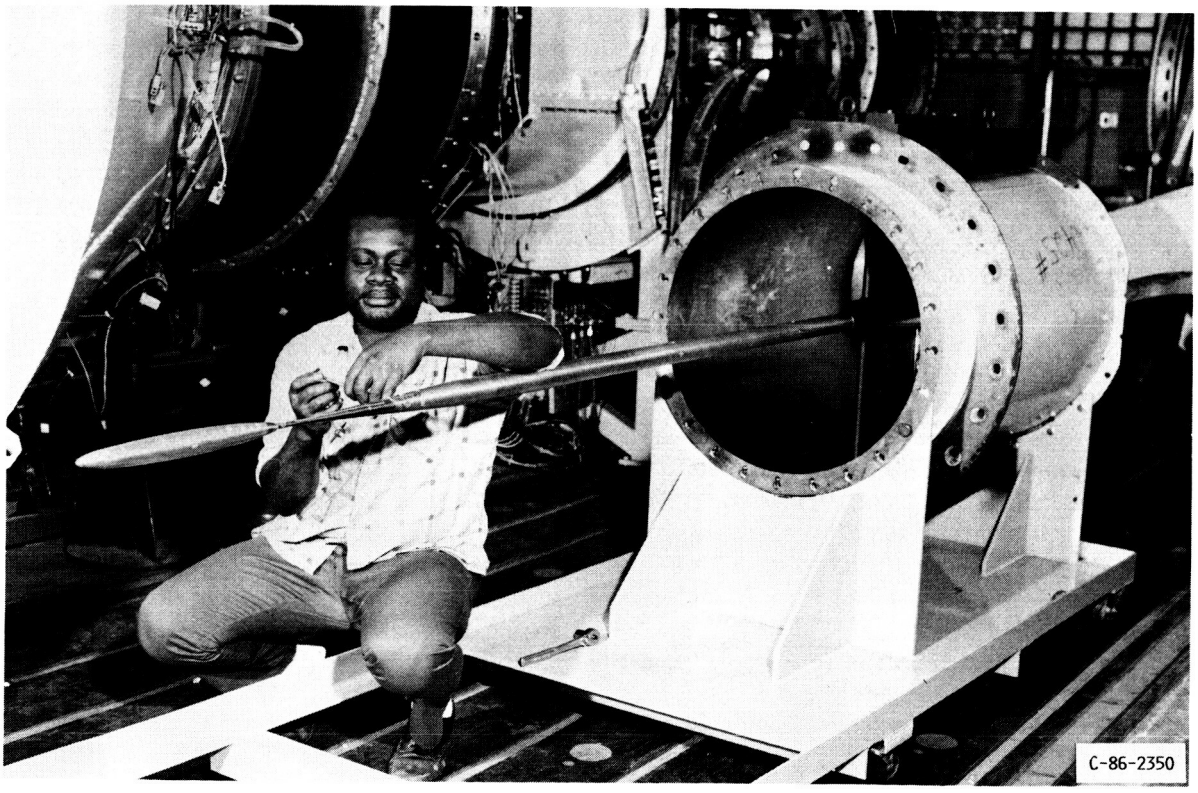


Figure 12.—0.43-Percent blockage model attached to sting supported by strut.

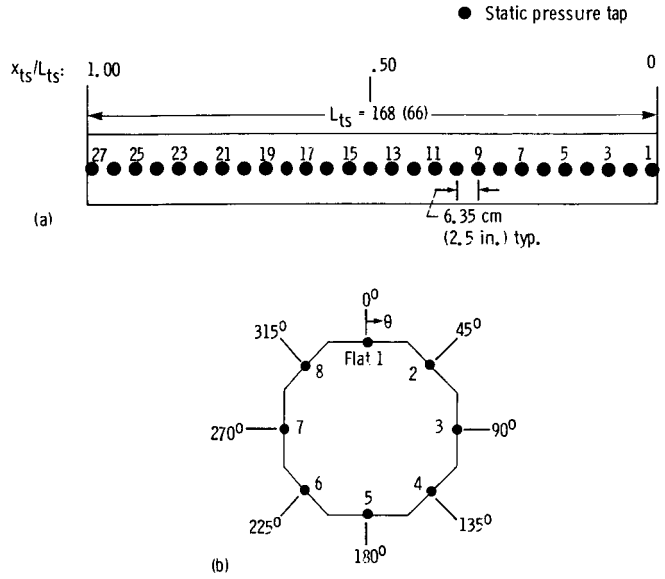


| Static pressure tap | Test-section axial location, $x_{ts}/L_{ts}$ | Static pressure tap | Test-section axial location, $x_{ts}/L_{ts}$ |
|---|---|---|---|
| 1 | 0.008 | 15 | 0.538 |
| 2 | .045 | 16 | .576 |
| 3 | .083 | 17 | .614 |
| 4 | .121 | 18 | .652 |
| 5 | .159 | 19 | .689 |
| 6 | .197 | 20 | .727 |
| 7 | .235 | 21 | .765 |
| 8 | .273 | 22 | .803 |
| 9 | .311 | 23 | .841 |
| 10 | .348 | 24 | .879 |
| 11 | .386 | 25 | .917 |
| 12 | .424 | 26 | .955 |
| 13 | .462 | 27 | .992 |
| (c) 14 | .500 | | |

(a) Axial locations.
(b) Circumferential locations (looking downstream).
(c) Instrumentation for flat 1 (typ. of eight).

Figure 13.—Test-section static pressure instrumentation.

### Procedure

All four blockage models were tested at 0° angle of attack and tunnel Mach numbers of 0.70, 0.80, 0.85, 0.90, 0.92, and 0.95. At each tunnel Mach number a range of PES flows was investigated, including zero PES flow where possible.

Test-section Reynolds number varied from $13.2\times10^6$ to $15.4\times10^6$ per meter ($4.0\times10^6$ to $4.7\times10^6$ per ft) for tunnel Mach numbers from 0.70 to 0.95.

The geometrically similar model in reference 13 had a boundary-layer transition strip located close to the nose. Each of the four blockage models used in the present investigation had a similar transition strip. However, during each run the grit wore off the strip because of the dirty air supply. Consequently it was not possible to artificially fix the location of boundary-layer transition.

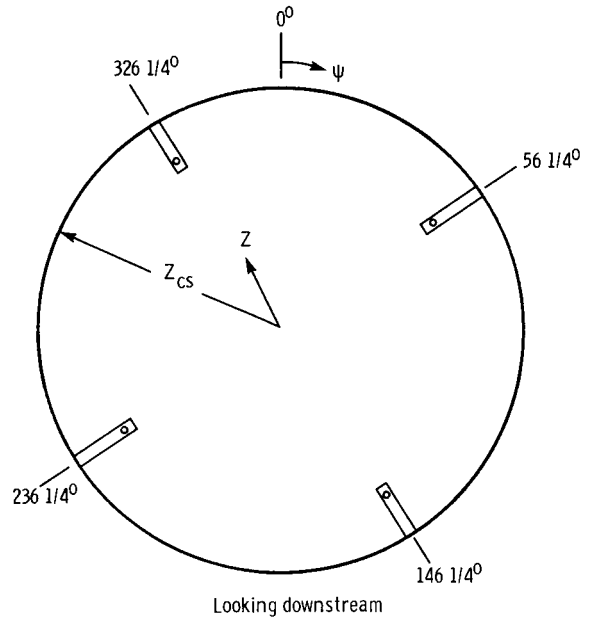


Figure 14.—Total pressure instrumentation at contraction-section entrance ($x_{ts}/L_{ts} = -0.851$). Radial location, $Z\angle Z_{cs}$, 0.877.

## Results and Discussion

### 0.43-Percent Blockage Model

With the 0.43-percent blockage model the pressure coefficient distribution over most of the model length, $0.142 \leqq x/L_R \leqq 0.854$, was essentially the same as the interference-free results (fig. 15) at all tunnel Mach numbers (0.70 to 0.95). Although slight differences existed between some measured pressure coefficients and the interference-free results, they corresponded to differences in tunnel Mach number of less than 0.9 percent at $x/L_R$ of 0.285, 0.570, and 0.783. This is probably within the accuracy that can be expected of pressure data taken on different models using different measurement systems in different wind tunnels. (As discussed later, the pressure coefficient distributions were not affected by the amount of PES flow, which was zero at Mach 0.70 to 0.92 and 1 percent at Mach 0.95.)

In two small regions the pressure coefficient distribution differed from the interference-free results.

(1) The static pressures near the aft section of the model ($0.854 \leq x/L_R \leq 0.961$) were somewhat greater than the interference-free results. This was possibly caused by a very small forward-facing step at $x/L_R = 0.970$, where the aft section fastened to the main section of the model. (The 0.43-percent blockage model was the only one constructed in this manner.) Downstream of $x/L_R = 0.970$ the static pressure distribution again was in good agreement with the interference-free results, indicating that the sting effect was essentially the same for both models.

(2) Just downstream of the model nose the measured pressure coefficient did not show the rapid expansion around the nose

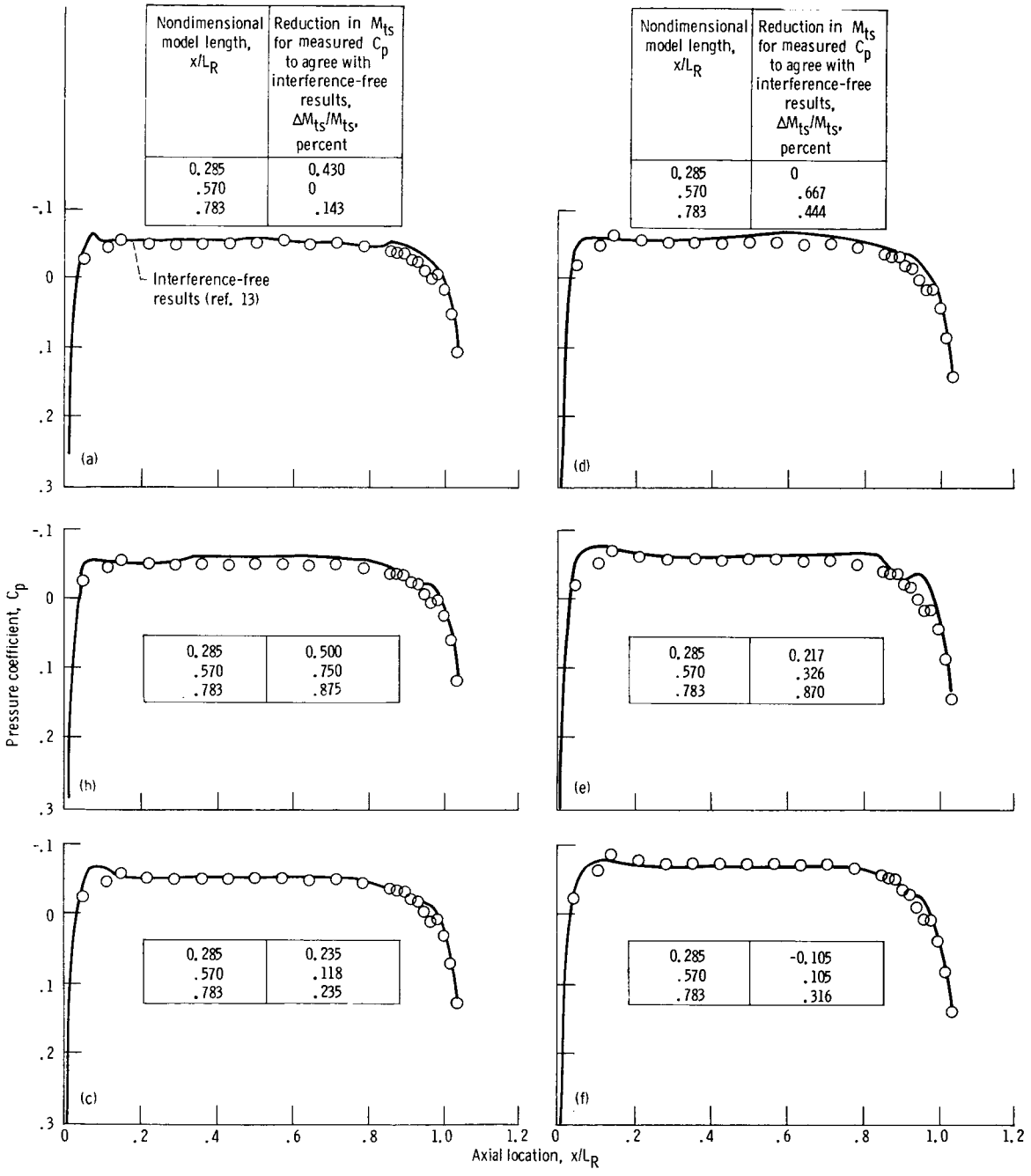


(a) Tunnel Mach number, $M_{ts}$, 0.70.
(b) Tunnel Mach number, $M_{ts}$, 0.80.
(c) Tunnel Mach number, $M_{ts}$, 0.85.
(d) Tunnel Mach number, $M_{ts}$, 0.90.
(e) Tunnel Mach number, $M_{ts}$, 0.92.
(f) Tunnel Mach number, $M_{ts}$, 0.95.

Figure 15.—Pressure distribution on 0.43-percent blockage model with no plenum evacuation system flow compared with interference-free results. Model nose at $x_{ts}/L_{ts} = 0.50$; reentry flaps at 9°; circumferential location of static pressure taps on model, $\varphi$, 0°.

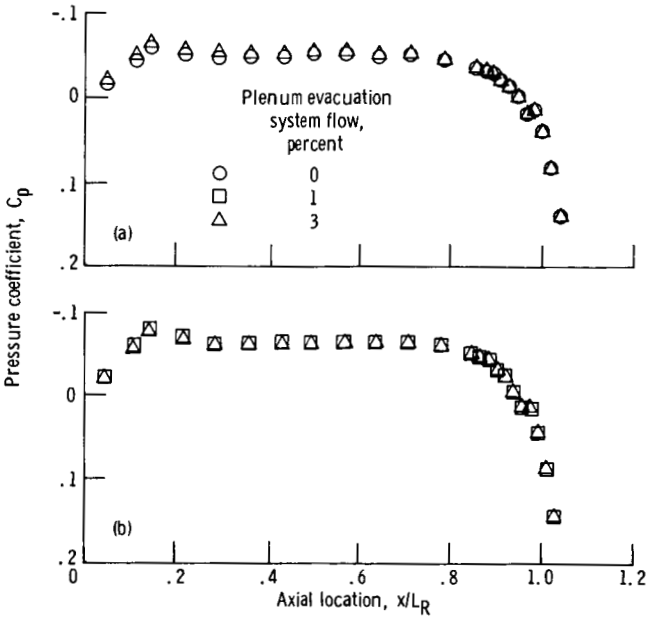


(a) Tunnel Mach number, $M_{ts}$, 0.90.
(b) Tunnel Mach number, $M_{ts}$, 0.95.

Figure 16.—Effect of plenum evacuation system flow on pressure coefficient distribution for 0.43-percent blockage model. Model nose at $x_{ts}/L_{ts} = 0.50$; reentry flaps at 9°; circumferential location of static pressure taps on model, $\varphi$, 0°.

that occurred on the geometrically similar model of reference 13. This might be due to small differences in the model contour near the nose, possibly caused by the grit transition strip used in reference 13. On the models of the present test, as already mentioned, the grit wore off during the run.

These small differences were not considered to be caused by wall interference. Consequently the pressure coefficient distribution on the 0.43-percent blockage model was considered to be free of tunnel wall effects and to be the same as the results in reference 13 except for the lack of rapid expansion around the model nose, as already mentioned. Therefore the data in subsequent figures for larger blockage models are compared with the results from reference 13 modified by eliminating the rapid expansion around the nose and replacing it with the pressure coefficient distribution of the 0.43-percent blockage model from the present tests.

For the 0.43-percent blockage model a change in PES flow, at least up to 3 percent, had no effect on the pressure distribution (fig. 16). This was true at all tunnel Mach numbers investigated.

The results just discussed were for the pressure coefficient distribution at the 0° circumferential location ($\varphi = 0°$). There was no circumferential variation in the pressure coefficients at seven of eight axial locations ($0.045 \le x/L_R \le 1.015$) for all tunnel Mach numbers (fig. 17). The small circumferential variation near the model nose at $x/L_R = 0.045$ was most likely due to a slight misalignment of the model with the tunnel centerline since at $x/L_R = 0.142$ the variation had disappeared.

The discussion so far has been concerned with pressure distributions on the model surface. The Mach number distribution on the test-section wall (fig. 18) was independent of circumferential location but was affected by the model as well as the sting support. Typically a mild increase in wall Mach number started at 4.5 percent into the test section ($x_{ts}/L_{ts} = 0.045$) and ended at the model nose ($x_{ts}/L_{ts} = 0.50$). The wall Mach number then increased somewhat more rapidly, reaching a peak at $x_{ts}/L_{ts} = 0.62$, at the model maximum diameter. It then decreased to a minimum at about $x_{ts}/L_{ts} = 0.80$, slightly downstream of the end of the minimum sting diameter. Thereafter the wall Mach number increased rapidly, reaching its maximum at the test-section exit. The rapid increase was due to a decrease in effective flow area caused by the increase in boundary-layer thickness on the test-section walls and on the sting in combination with the increase in the sting diameter, which reached its maximum at the test-section exit.

The effect of the blockage model and the sting on wall Mach number became more pronounced with increasing tunnel Mach number $M_{ts}$. At $M_{ts} = 0.70$ (fig. 18(a)) the effect was barely noticeable except near the exit of the slotted test section ($x_{ts}/L_{ts} \approx 1.0$), where the minimum effective flow area occurred. However, at $M_{ts} = 0.90$ (fig. 18(c)) the effect was very evident. The flow was almost choked at the exit of the slotted test section, so that this was about the highest tunnel Mach number that could be achieved with no PES flow. (An $M_{ts}$ of 0.92 was the highest achieved without PES flow.) A PES flow of 1 percent of the tunnel flow was required to achieve an $M_{ts}$ of 0.95. At this tunnel Mach number (fig. 18(d)) the flow choked at about $x_{ts}/L_{ts} = 0.89$. Choking occurred at this location because the PES flow was greater than required to achieve a flat axial wall Mach number distribution (ref. 11). Consequently the wall Mach numbers near the exit of the test section were reduced, causing the minimum effective flow area to move upstream from the test-section exit.

Thus the wall Mach number distribution was affected by the blockage model and the sting support. The effect of the sting was sufficiently large that, combined with the boundary-layer buildup on the walls of the slotted test section and on the sting, it resulted in a limit on the highest tunnel Mach number that could be achieved without using PES flow.

### 3-Percent Blockage Model

The nose of the 3-percent blockage model was located midway into the test section ($x_{ts}/L_{ts} = 0.50$), and consequently the model was too long to be contained within the test section. The model length at the test-section exit nondimensionalized by the reference length was $x/L_R = 0.871$. With no PES flow the tunnel walls affected the pressure coefficient distribution over almost the entire length of the model for all tunnel Mach numbers investigated (fig. 19). Only pressures near the model

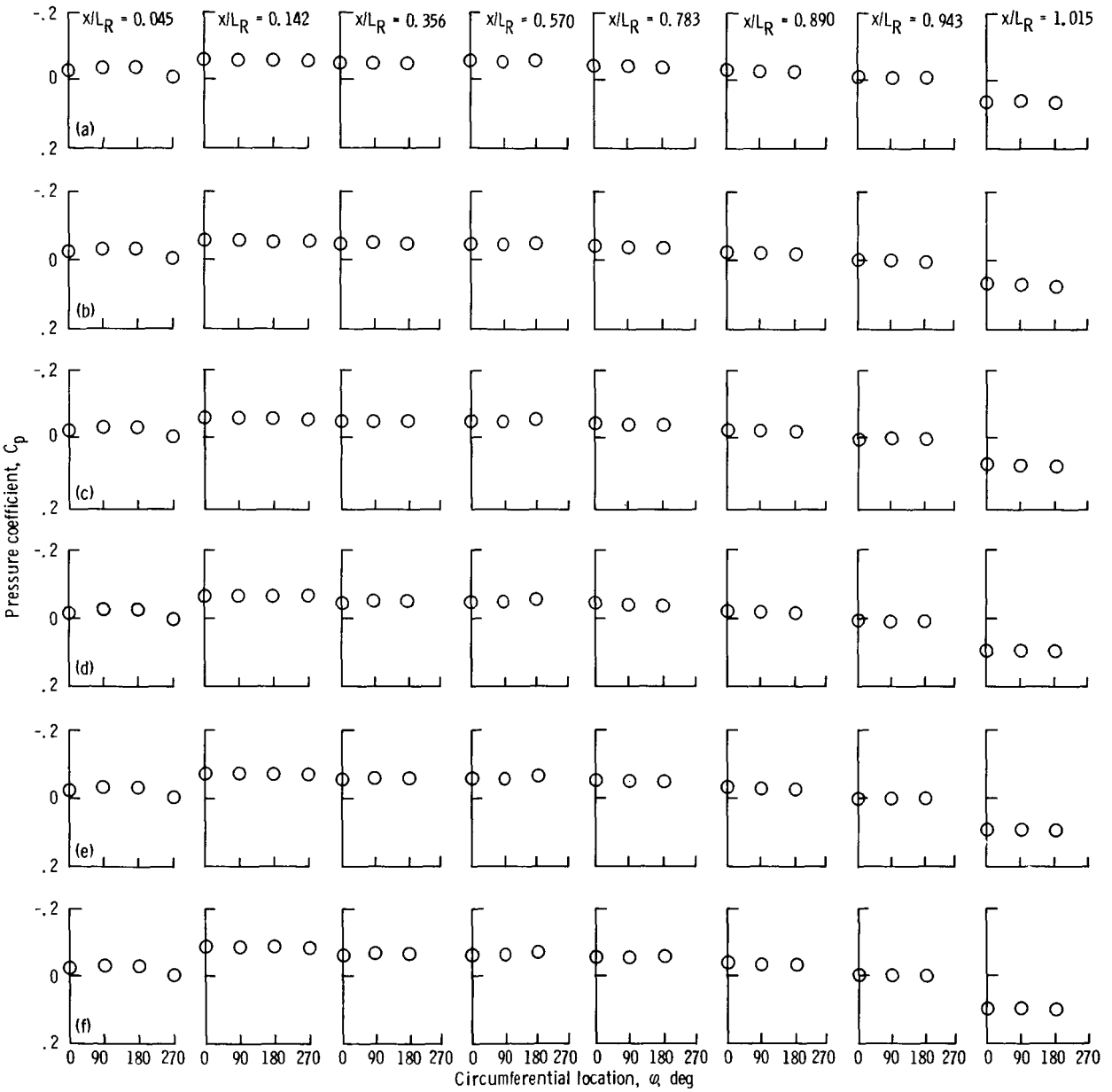


(a) Tunnel Mach number, $M_{ts}$, 0.70.
(b) Tunnel Mach number, $M_{ts}$, 0.80.
(c) Tunnel Mach number, $M_{ts}$, 0.85.
(d) Tunnel Mach number, $M_{ts}$, 0.90.
(e) Tunnel Mach number, $M_{ts}$, 0.92.
(f) Tunnel Mach number, $M_{ts}$, 0.95.

Figure 17.—Effect of circumferential location on pressure coefficient distribution for 0.43-percent blockage model. Model nose at $x_{ts}/L_{ts} = 0.50$; no plenum evacuation system flow; reentry flaps at 9°.

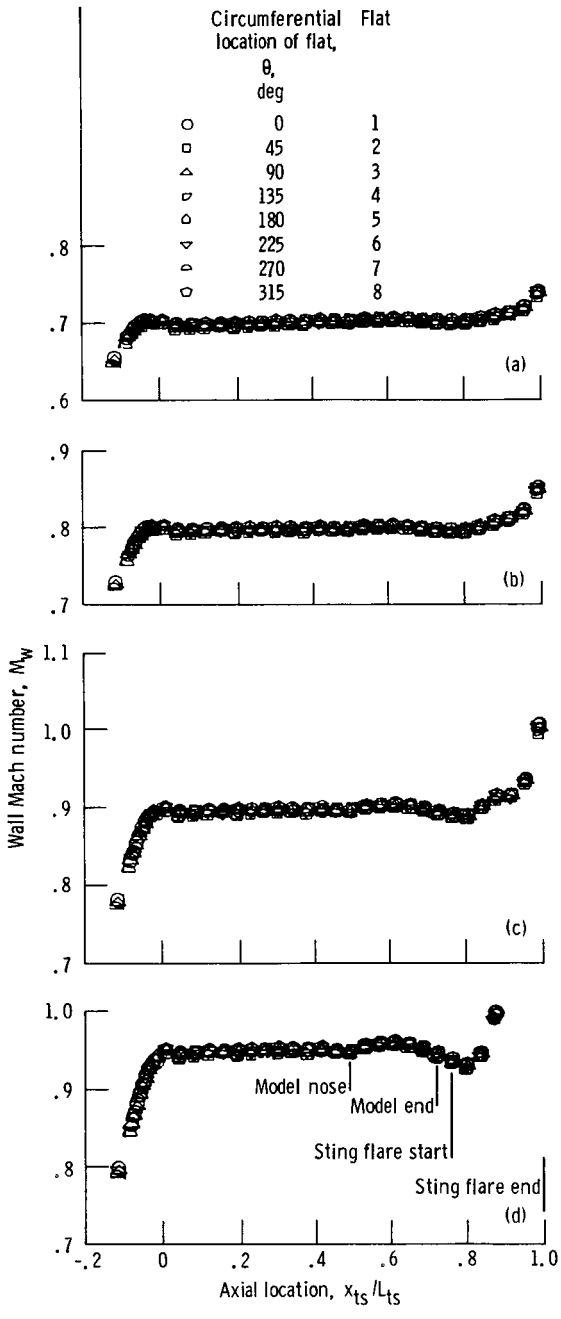


(a) Tunnel Mach number, $M_{ts}$, 0.70; no PES flow.
(b) Tunnel Mach number, $M_{ts}$, 0.80; no PES flow.
(c) Tunnel Mach number, $M_{ts}$, 0.90; no PES flow.
(d) Tunnel Mach number, $M_{ts}$, 0.95; 1-percent PES flow.

Figure 18.—Test-section wall Mach number distribution with 0.43-percent model installed. Model nose at $x_{ts}/L_{ts} = 0.50$; reentry flaps at 9°.

nose ($x/L_R = 0.107$) were not affected by the tunnel walls. Downstream of this location, however, the pressure increased until it became somewhat greater than the interference-free results and stayed at this level over the remainder of the forward half of the model (i.e., up to $x/L_R = 0.50$). Then the pressure decreased fairly rapidly, with the minimum value, which was considerably lower than the interference-free results, occurring near the test-section exit. From the test-section exit to the end of the model, pressure increased steeply. Thus for no PES flow the tunnel walls caused the pressures over most of the forward half of the model to be somewhat higher than the interference-free results and those over the aft part of the model inside the test section to be considerably lower than the interference-free results.

Increasing the tunnel Mach number resulted in only a small increase in the pressures on the forward half of the model but a considerable decrease in the pressures on the aft part of the model inside the test section. For example, at $x/L_R$ of 0.356 and 0.872 the pressure coefficients were −0.045 and −0.11, respectively, at $M_{ts} = 0.70$ (fig. 19(a)) and −0.046 and −0.187, respectively, at $M_{ts} = 0.95$ (fig. 19(f)).

PES flow influenced the pressure distribution only on the aft part of the model. When the PES flow was increased to an appropriate value, interference-free results were achieved over the aft part of the model. Increasing the tunnel Mach number increased the amount of PES flow required to achieve interference-free results. For example, at $M_{ts} = 0.70$ (fig. 19(a)) a PES flow of 1.40 percent of the main flow was required to achieve interference-free results for model locations downstream of $x/L_R = 0.712$. At $M_{ts} = 0.95$ (fig. 19(f)), however, a PES flow of 2.25 percent of the main flow was required to achieve interference-free results. More will be said about this later.

As mentioned, pressures on the forward half of the model were higher than the interference-free results and slightly increased with increasing tunnel Mach number. This can be explained with the aid of figure 20, which presents the test-section wall Mach number circumferential and axial distributions. There was no circumferential distribution. The axial distribution was fairly flat except for two regions. At the test-section exit the Mach number increased because of boundary-layer thickening. Halfway into the test section, at $x_{ts}/L_{ts} = 0.50$, the Mach number decreased. This Mach number decrement was caused by the test-section open area ratio being too large (11 percent). This allowed too much of the tunnel flow to exit the test section through the eight longitudinal slots, thereby decreasing the flow and consequently the Mach number over the forward part of the model. This in turn increased the surface pressures on the model.

Figure 20 also shows that the magnitude of the test-section wall Mach number decrement increased with increasing tunnel Mach number. For example, at $M_{ts} = 0.80$ (fig. 20(b)) the wall Mach number at $x_{ts}/L_{ts} = 0.50$ decreased from 0.80 to 0.785, but at $M_{ts} = 0.95$ (fig. 20(d)) this wall Mach number decreased from 0.95 to 0.93. Thus increasing the tunnel Mach number allowed a greater percentage of the flow to exit the test section, thereby further reducing the flow and Mach number over the forward part of the model. This further increased the model surface pressures. Thus in the region where the forward part of the model was located, the slotted test section was functioning as a free-jet wind tunnel (ref. 15).

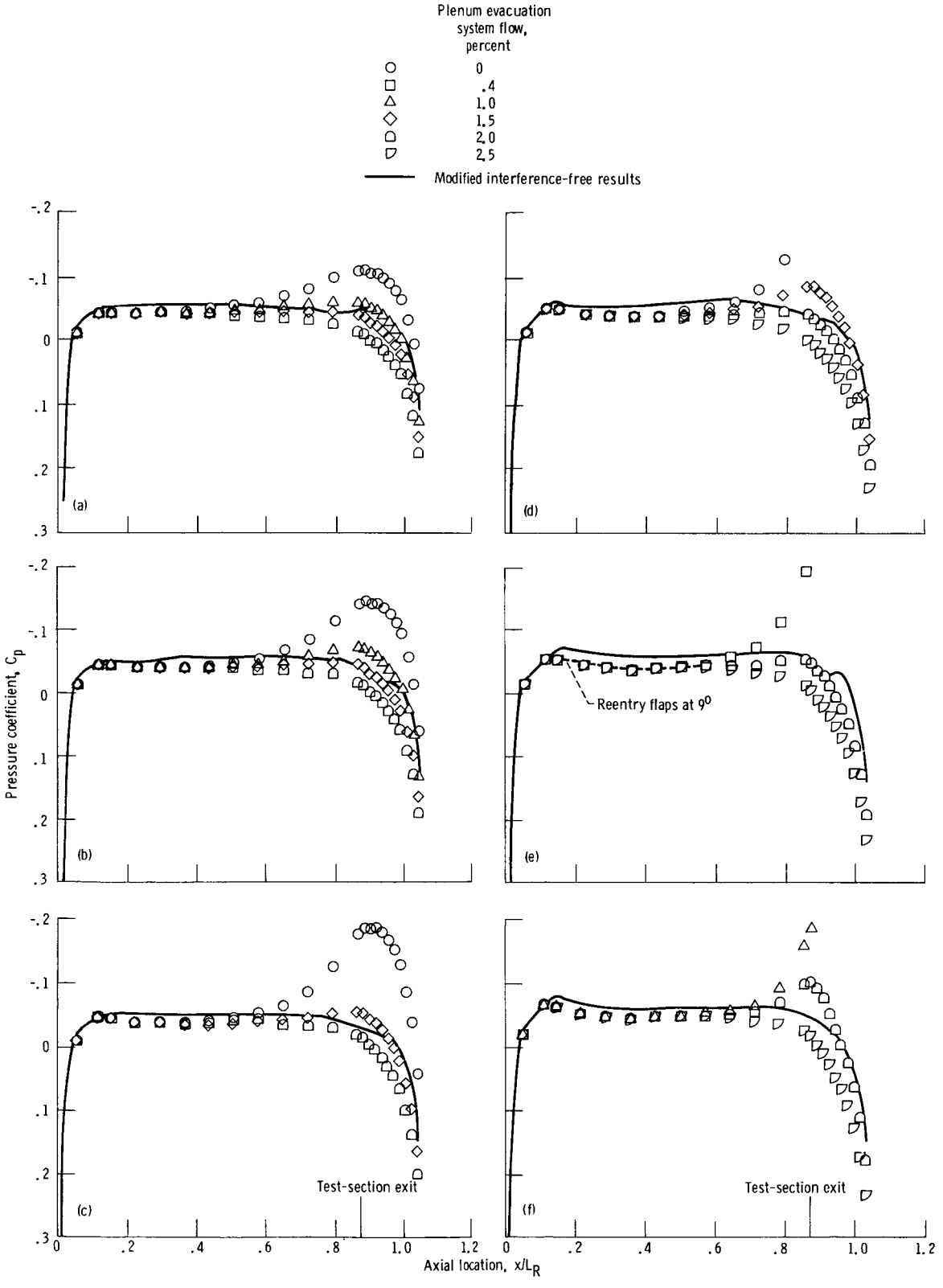


(a) Tunnel Mach number, $M_{ts}$, 0.70.
(b) Tunnel Mach number, $M_{ts}$, 0.80.
(c) Tunnel Mach number, $M_{ts}$, 0.85.
(d) Tunnel Mach number, $M_{ts}$, 0.90.
(e) Tunnel Mach number, $M_{ts}$, 0.92.
(f) Tunnel Mach number, $M_{ts}$, 0.95.

Figure 19.—Effect of plenum evacuation system flow on pressure coefficient distribution for 3-percent blockage model. Model nose at $x_{ts}/L_{ts} = 0.50$; reentry flaps at 9°; circumferential location of static pressure taps on model, $\varphi$, 0°.

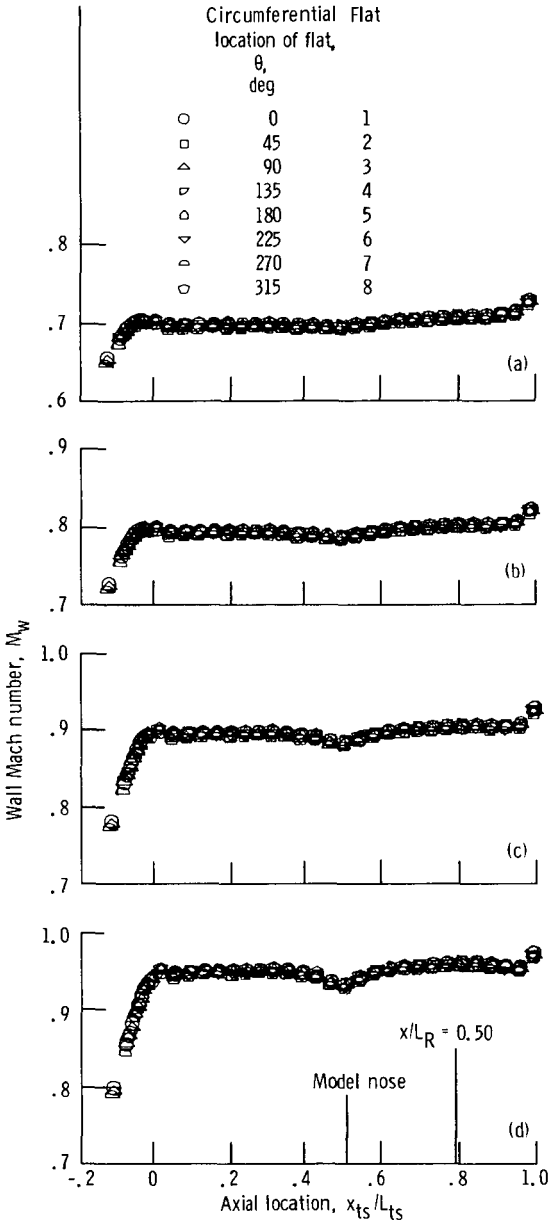


(a) Tunnel Mach number, $M_{ts}$, 0.70.
(b) Tunnel Mach number, $M_{ts}$, 0.80.
(c) Tunnel Mach number, $M_{ts}$, 0.90.
(d) Tunnel Mach number, $M_{ts}$, 0.95.

Figure 20.—Test-section wall Mach number distribution with 3-percent blockage model installed. Model nose at $x_{ts}/L_{ts} = 0.50$; reentry flaps at 9°.

On the basis of the preceding discussion, interference-free results can be achieved on the aft part of the model by selecting the proper ratio of PES flow to tunnel flow. No adjustment to the width of the eight longitudinal slots would be required in the region where the aft part of the blockage model was located. Achieving interference-free results on the forward part of the model, where PES flow has no influence, however, would require narrowing the slots in the region where the forward part of the model was located. Achieving interference-free results over the entire range of tunnel Mach numbers investigated would require that the width of the longitudinal slots, along with the PES flow, change with changes in tunnel Mach number. As the tunnel Mach number increases, the width of the slots must decrease and the ratio of PES flow to tunnel flow must increase.

## 6-Percent Blockage Model

The nose of the 6-percent blockage model was located at $x_{ts}/L_{ts} = 0.18$ so that almost the entire length of the model would be contained within the test section. The model nondimensional length at the test-section exit was $x/L_R = 1.008$. The axial pressure coefficient distribution on the 6-percent blockage model (fig. 21) was similar to that on the 3-percent blockage model with one exception. The very rapid expansion of the flow around the model nose, which also occurred on the 3-percent blockage model, was followed by a fairly rapid compression and then an expansion that was not significant on the 3-percent model. The compression region on the 6-percent blockage model extended from about $x/L_R = 0.107$ to $x/L_R = 0.214$. The magnitude of this compression was not significantly affected by changes in tunnel Mach number; the maximum values of the pressure coefficient were $-0.021$ at $M_{ts} = 0.70$ (fig. 21(a)) and $-0.023$ at $M_{ts} = 0.95$ (fig. 21(f)). However, the magnitude of the expansion was significantly affected by changes in tunnel Mach number, with the flow expanding to a lower pressure as the tunnel Mach number increased. At $x/L_R = 0.356$, which was the end of the expansion, the pressure coefficient was $-0.026$ at $M_{ts} = 0.70$ (fig. 21(a)) but $-0.048$ at $M_{ts} = 0.95$ (fig. 21(f)). In the compression and expansion regions the pressures were higher than the interference-free results. These pressures were not significantly influenced by PES flow over the entire range of tunnel Mach numbers investigated.

PES flow again influenced the axial pressure coefficient distribution only on the aft part of the model. However, a greater ratio of PES flow to tunnel flow was required to achieve interference-free results on the aft part of the 6-percent model than on the aft part of the 3-percent model. Increasing the tunnel Mach number again increased the amount of PES flow required. The ratios of PES flow to tunnel flow required to achieve interference-free results at $M_{ts}$ of 0.70 and 0.95 were 1.9 and 3.8 percent, respectively (figs. 21(a) and (f)).

With the 6-percent blockage model there was no circumferential variation in the wall Mach number distribution (fig. 22). The axial distribution was similar to that with the 3-percent blockage model; that is, the decrement in wall Mach number again occurred near the axial location of the model nose. The magnitude and extent of this decrement, however, were larger with the 6-percent than with the 3-percent blockage model. (For example, compare fig. 20(d) with fig. 22(d).) This means that, for the same tunnel Mach number, more flow exited the slotted test section with the 6-percent than with the 3-percent blockage model, resulting in higher surface pressures on the forward part of the 6-percent model.

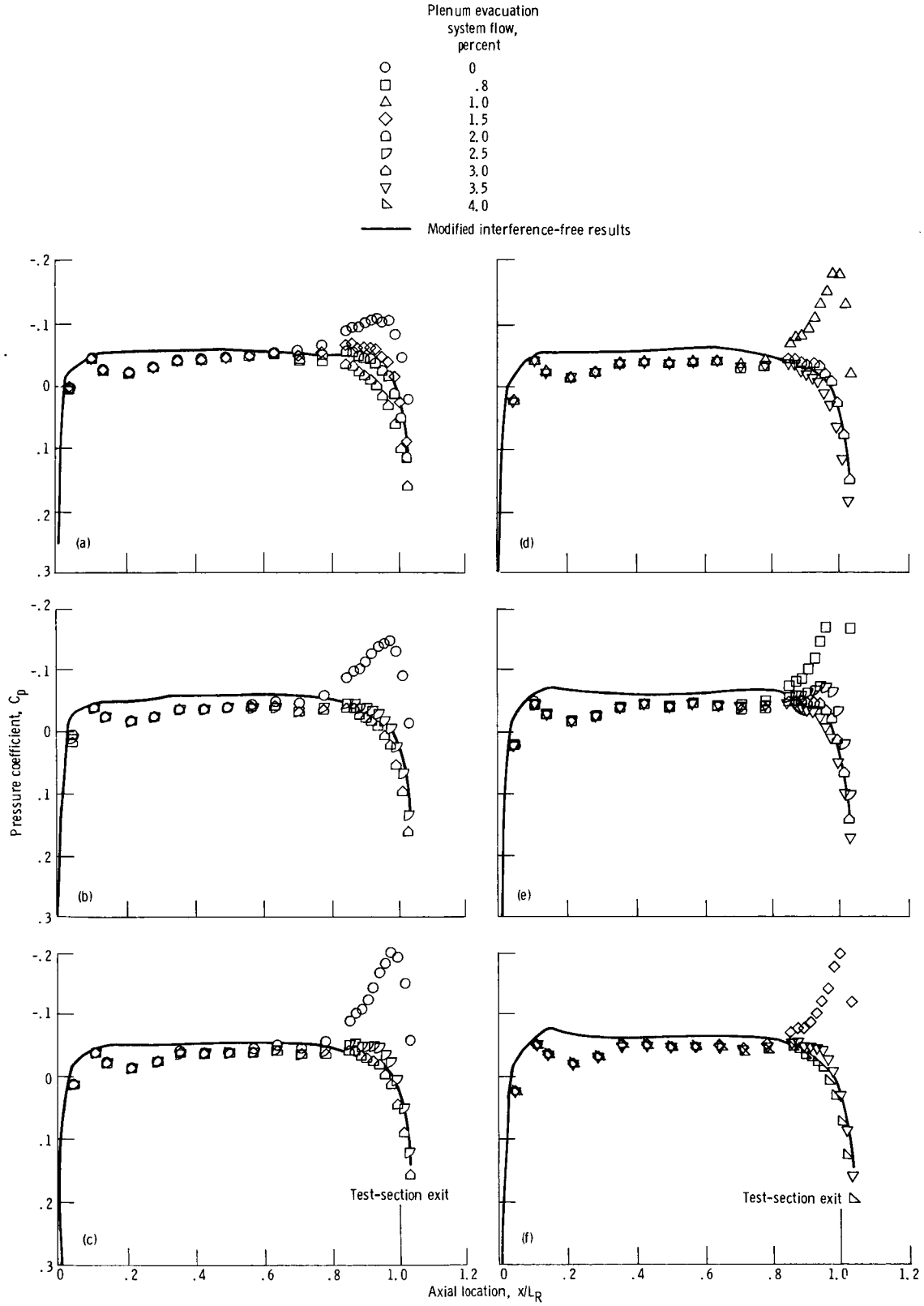


(a) Tunnel Mach number, $M_{ts}$, 0.70.
(b) Tunnel Mach number, $M_{ts}$, 0.80.
(c) Tunnel Mach number, $M_{ts}$, 0.85.
(d) Tunnel Mach number, $M_{ts}$, 0.90.
(e) Tunnel Mach number, $M_{ts}$, 0.92.
(f) Tunnel Mach number, $M_{ts}$, 0.95.

Figure 21.—Effect of plenum evacuation system flow on pressure coefficient distribution for 6-percent blockage model. Model nose at $x_{ts}/L_{ts} = 0.18$; reentry flaps at 9°; circumferential location of static pressure taps on model, $\varphi$, 0°.

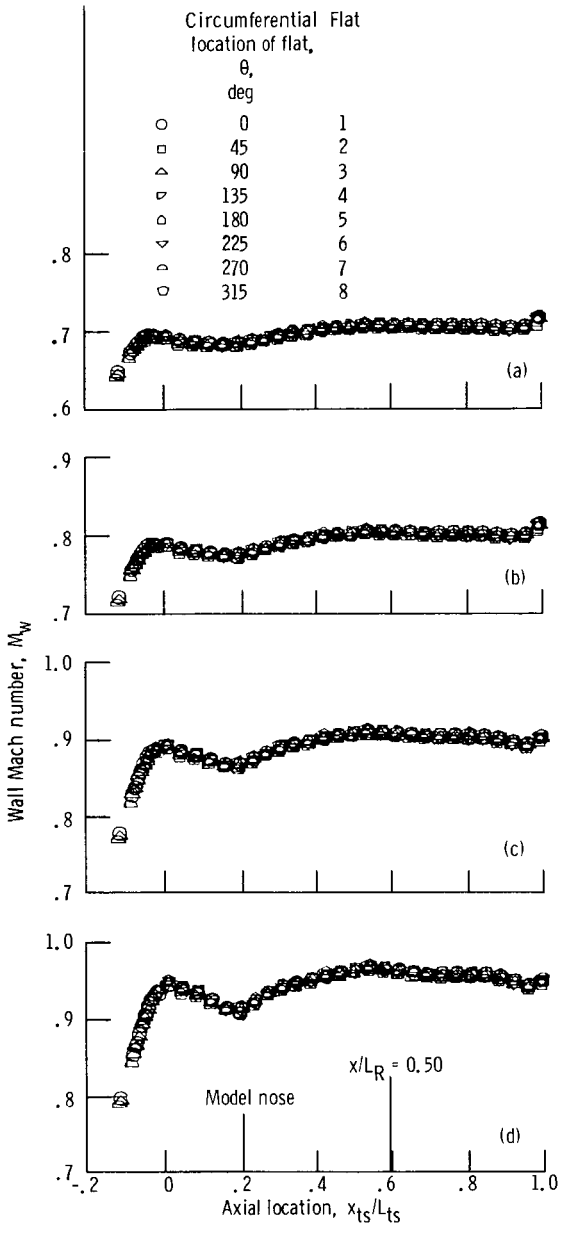


(a) Tunnel Mach number, $M_{ts}$, 0.70.
(b) Tunnel Mach number, $M_{ts}$, 0.80.
(c) Tunnel Mach number, $M_{ts}$, 0.90.
(d) Tunnel Mach number, $M_{ts}$, 0.95.

Figure 22.—Test-section wall Mach number distribution with 6-percent model installed. Model nose at $x_{ts}/L_{ts} = 0.18$; reentry flaps at 9°.

The large magnitude and extent of the decrement in tunnel wall Mach number near the nose of the 6-percent blockage model along with the compression and expansion region on this model suggest that the test-section slot width geometry should be different in this region of the model. The 6-percent model was located closer to the test-section entrance than the two previous models discussed ($x_{ts}/L_{ts} = 0.18$ vs 0.50). Since slot width decreased from its maximum value at $x_{ts}/L_{ts} = 0.18$ to zero at the test-section entrance, this might affect the model pressures. However, as discussed later, model axial location had no significant effect on model pressure distribution in this region. Thus the model pressure distribution most likely was due to the width of the eight longitudinal slots being constant at $x_{ts}/L_{ts} > 0.18$. To achieve interference-free results, slot width should vary in the region of the model where compression and expansion occur. Qualitatively, in the compression region the slot width should decrease to a minimum where the maximum model pressure occurs ($x_{ts}/L_{ts} = 0.214$). Then as the flow expands, the slot width should increase to a maximum where the pressure becomes constant ($x_{ts}/L_{ts} = 0.471$). The maximum width, however, should be less than that associated with the 3-percent model. Slot geometry should be the same for all tunnel Mach numbers, but slot width should decrease with increasing tunnel Mach number.

Thus installing the 6-percent model rather than the 3-percent model in the slotted test section had two effects. A major effect was that a change in the test-section slot width geometry was required in the region where the forward part of the 6-percent model was located and where PES flow had no influence. The other effect was on the aft part of the model, where PES flow had an influence. The 6-percent model required more PES flow to achieve interference-free results than the 3-percent model.

As already mentioned, the nose of the 6-percent blockage model was located at $x_{ts}/L_{ts} = 0.18$ so that almost the entire model length could be accommodated within the test section. This was also the farthest upstream location at which the longitudinal slots in the test section had their full width. Farther upstream the slots narrowed linearly until they were completely closed at the test-section entrance. This slot geometry might affect the pressure coefficient distribution on the forward part of the model, in particular the region $0.107 \le x/L_R \le 0.356$, where the flow over the model compressed and then expanded. To investigate this, the model was moved downstream so that its nose was located midway into the test section at $x_{ts}/L_{ts} = 0.50$, where the noses of the 0.43-percent and 3-percent blockage models had been located. This resulted in about 42 percent of the 6-percent blockage model length extending downstream from the test-section exit. Thus the pressure coefficient distribution from $x/L_R = 0.616$ to the end of the model would not be indicative of the results achieved in the slotted test section, but the region of interest ($x/L_R < 0.356$) would be.

With the 6-percent blockage model nose located at $x_{ts}/L_{ts} = 0.50$, increasing the PES flow had only a small influence on the model pressure distribution in the region where the flow over the model compressed and then expanded ($0.107 \le x/L_R \le 0.356$) at $M_{ts} = 0.70$ and had no significant influence at $M_{ts}$ of 0.90 and 0.95 (fig. 23). The pressure distribution in this region was essentially the same as when the model was located at $x_{ts}/L_{ts} = 0.18$. Therefore this pressure distribution was not due to the increase in slot width from closed at the entrance to fully open at 18 percent into the test section ($x_{ts}/L_{ts} = 0.18$). It was most likely due to improper slot width geometry, as already discussed.

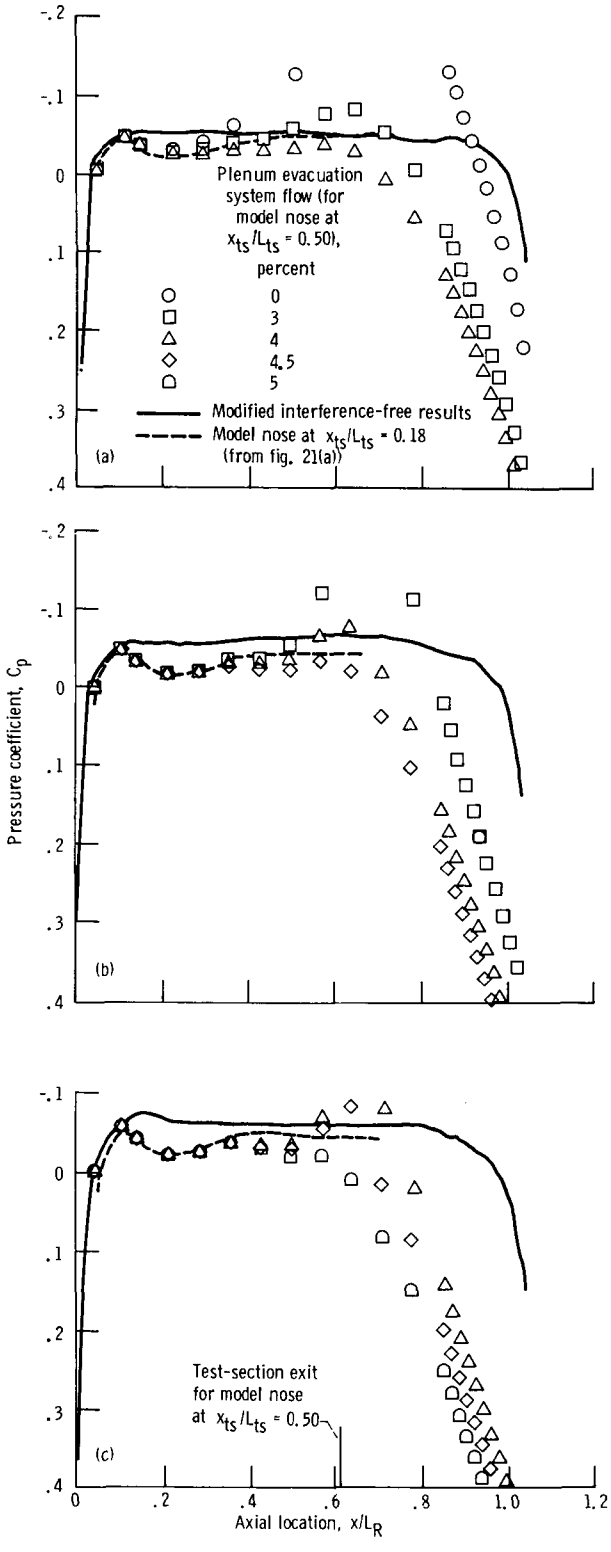


(a) Tunnel Mach number, $M_{ts}$, 0.70.
(b) Tunnel Mach number, $M_{ts}$, 0.90.
(c) Tunnel Mach number, $M_{ts}$, 0.95.

Figure 23.—Effect of model axial location in test section on pressure coefficient distribution for 6-percent blockage model. Reentry flaps at 9°; circumferential location of static pressure taps on model, $\varphi$, 0°.

## 12-Percent Blockage Model

The nose of the 12-percent blockage model was located at $x_{ts}/L_{ts} = 0.18$ so that as much as possible of the model would be contained within the test section. The model nondimensional length at the test-section exit was $x/L_R = 0.713$. This model was very long, and even with its nose at $x_{ts}/L_{ts} = 0.18$ about 32 percent of its actual length

$$\frac{(79.81 - 0.713 \times 75.78)}{79.81} \times 100 = 32 \text{ percent}$$

extended downstream from the test-section exit. Thus the pressure coefficient axial distribution downstream of $x/L_R = 0.713$ was not indicative of what would be achieved in the slotted test section (fig. 24). Moreover the large size of this model restricted the amount of useful information that could be obtained.

Results with no PES flow could be obtained only at the lowest tunnel Mach number investigated ($M_{ts} = 0.70$). Higher tunnel Mach numbers required some PES flow to eliminate the choking that otherwise would have occurred at the test-section exit because of the combination of a very large model cross section and thickening of the boundary layer on the tunnel walls and model. Relatively large amounts of PES flow, between 7 and 9 percent of the tunnel flow, were required to achieve the higher tunnel Mach numbers. Also, it was not possible to determine the value of PES flow required to achieve interference-free results because at $M_{ts} \geq 0.80$, PES flow influenced just a very small length of the model inside the test section. At $0.80 \leq M_{ts} \leq 0.90$, PES flow influenced only about 20 percent of the model length inside the test section; at $M_{ts}$ of 0.92 and 0.95, PES flow influenced only about 10 percent of the model length inside the test section.

The useful information that was obtained pertained to the pressure coefficient distribution on the forward part of the model, which was not influenced by PES flow. Flow expansion around the nose of this model was considerably less than for the 6-percent model. Thus high pressure extended farther upstream on the 12-percent model than on the 6-percent model. Downstream of the flow expansion around the nose was a compression region centered at about $x/L_R = 0.498$. The compression region was farther downstream on the 12-percent model than on the 6-percent model. Pressure on the entire forward part of the 12-percent model also was very much greater than interference-free results over the entire range of tunnel Mach numbers investigated.

With the 12-percent blockage model, as with the 3- and 6-percent models, there was no variation in the circumferential distribution, and the axial distribution exhibited a decrement in wall Mach number near the nose (fig. 25). The magnitude and extent of this decrement, which increased with increasing tunnel Mach number, were much larger than those associated

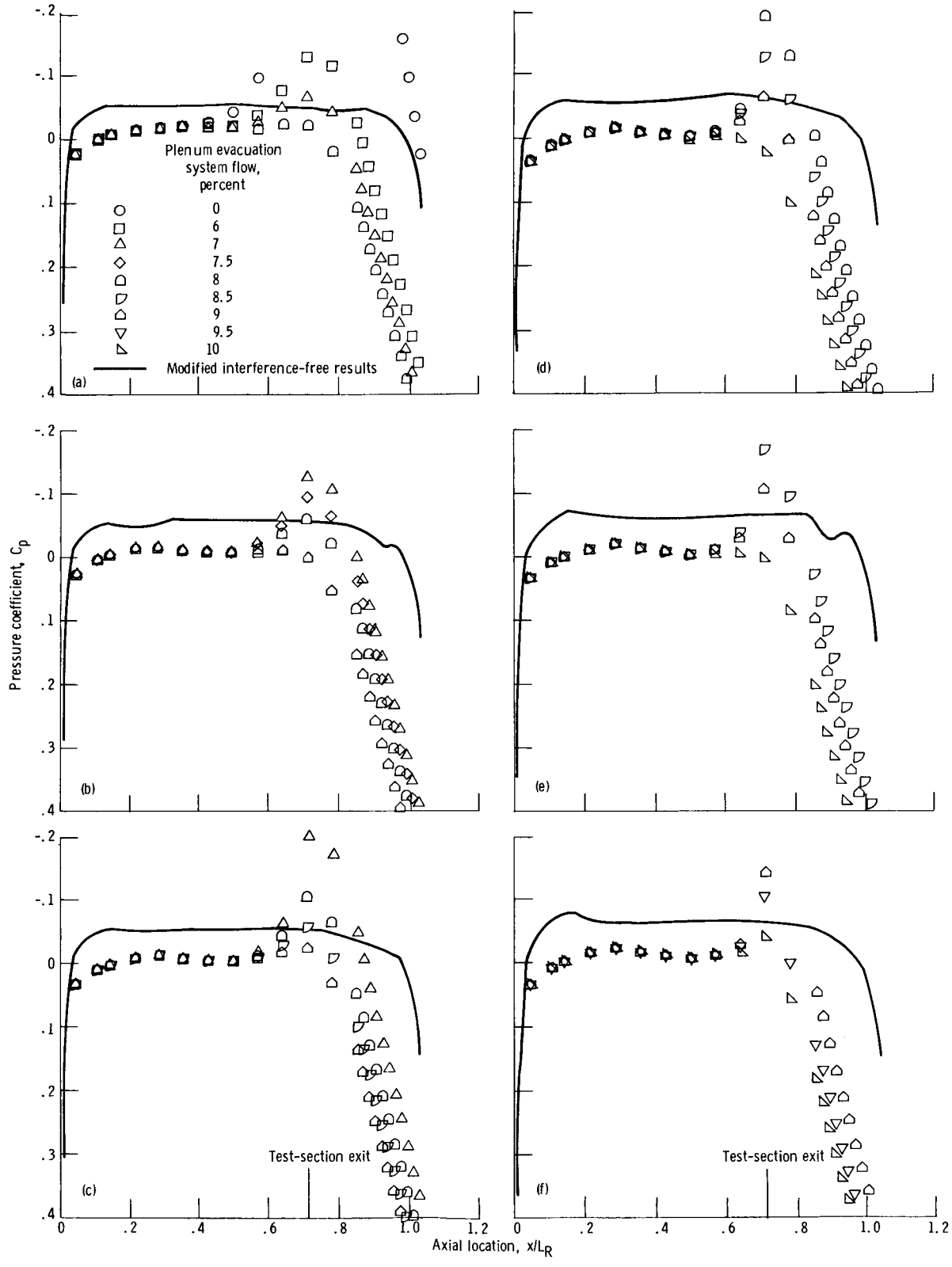


(a) Tunnel Mach number, $M_{ts}$, 0.70.
(b) Tunnel Mach number, $M_{ts}$, 0.80.
(c) Tunnel Mach number, $M_{ts}$, 0.85.
(d) Tunnel Mach number, $M_{ts}$, 0.90.
(e) Tunnel Mach number, $M_{ts}$, 0.92.
(f) Tunnel Mach number, $M_{ts}$, 0.95.

Figure 24.—Effect of plenum evacuation system flow on pressure coefficient distribution for 12-percent blockage model. Model nose at $x_{ts}/L_{ts} = 0.18$; reentry flaps at 9°; circumferential location of static pressure taps on model, $\varphi$, 0°.

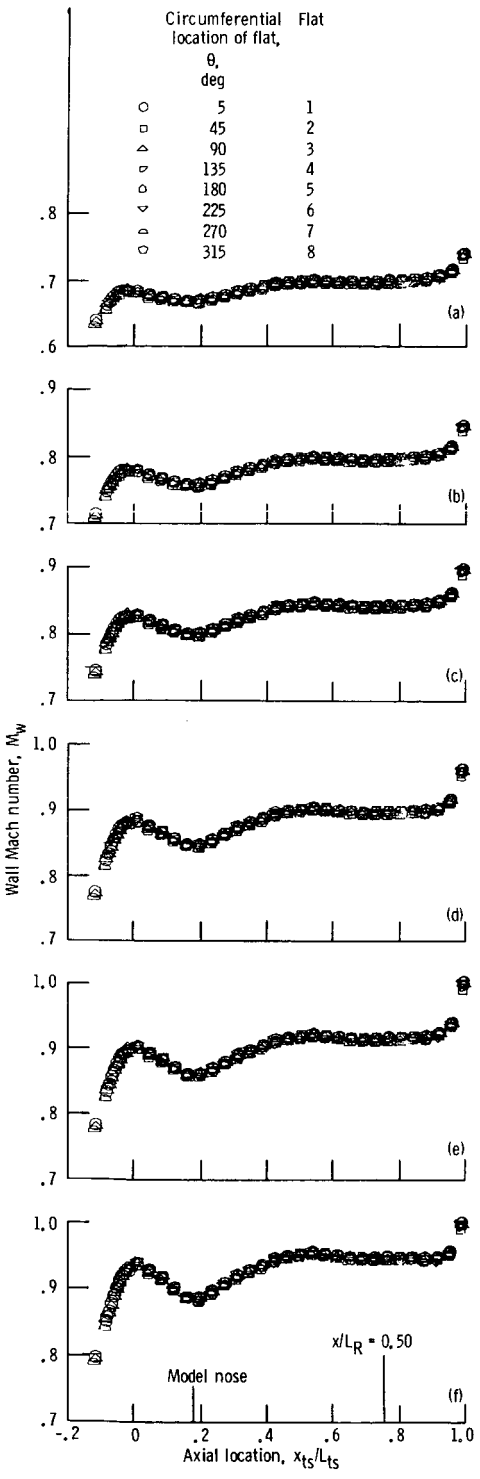


(a) Tunnel Mach number, $M_{ts}$, 0.70; PES flow, 7 percent.
(b) Tunnel Mach number, $M_{ts}$, 0.80; PES flow, 8 percent.
(c) Tunnel Mach number, $M_{ts}$, 0.85; PES flow, 8.5 percent.
(d) Tunnel Mach number, $M_{ts}$, 0.90; PES flow, 9 percent.
(e) Tunnel Mach number, $M_{ts}$, 0.92; PES flow, 9 percent.
(f) Tunnel Mach number, $M_{ts}$, 0.95; PES flow, 10 percent.

Figure 25.—Test-section wall Mach number distribution with 12-percent model installed. Model nose at $x_{ts}/L_{ts} = 0.18$; reentry flaps at 9°.

with the 6-percent blockage model. Thus there was a greater decrease in Mach number over the 12-percent model than over the 6-percent model. This resulted in higher surface pressures on the forward part of the 12-percent model than on the 6-percent model.

The previous discussion indicated that, compared with the forward part of the 6-percent model, not only were the pressures higher on the forward part of the 12-percent model, but the high pressure extended farther upstream and the compression region occurred farther downstream. This implies that, to achieve interference-free results, the width, extent, and shape of the eight longitudinal slots should be different with the 12-percent model installed in the test section. The 12-percent model requires narrower slots extending farther upstream. Also, the slot width should vary where the flow expanded around the model nose as well as where compression occurred. In the expansion region the slot width should increase to a maximum at $x_{ts}/L_{ts} = 0.51$, where minimum pressure occurred on the forward part of the model. Then the slot width should decrease to a minimum at $x_{ts}/L_{ts} = 0.754$, where maximum pressure occurred on the forward part of the model.

## Optimum Plenum Evacuation System Flow

As has already been mentioned, a particular ratio of plenum evacuation system flow to tunnel flow was required to achieve

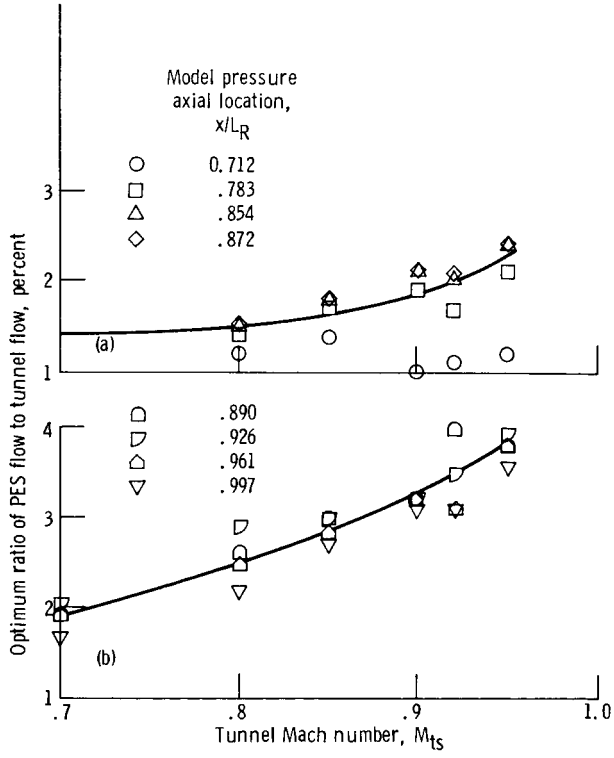


(a) 3-Percent blockage model; model nose at $x_{ts}/L_{ts} = 0.50$.
(b) 6-Percent blockage model; model nose at $x_{ts}/L_{ts} = 0.18$.

Figure 26.—Effect of tunnel Mach number and model blockage on optimum plenum evacuation system flow. Reentry flaps at 9°.

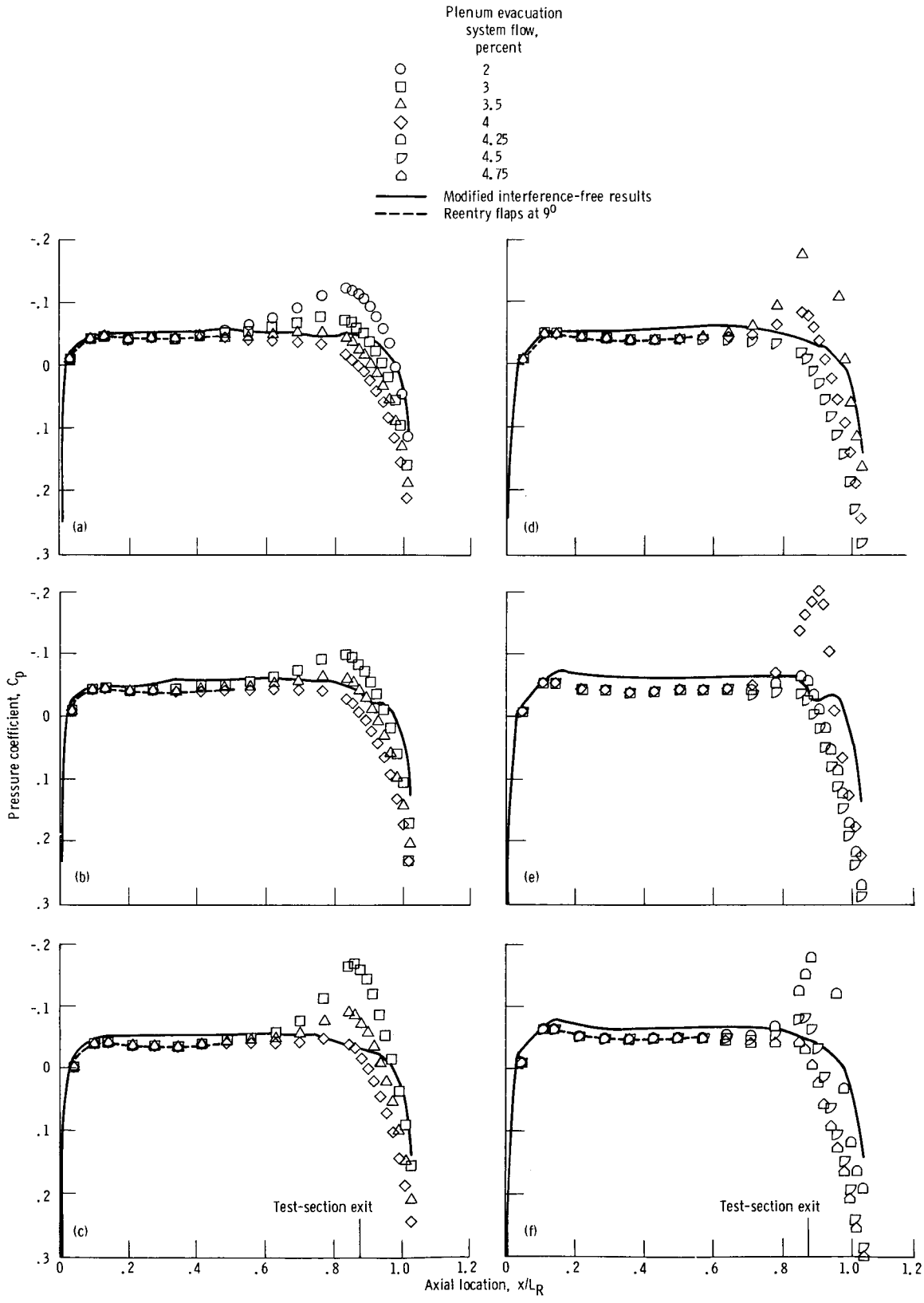


(a) Tunnel Mach number, $M_{ts}$, 0.70.
(b) Tunnel Mach number, $M_{ts}$, 0.80.
(c) Tunnel Mach number, $M_{ts}$, 0.85.
(d) Tunnel Mach number, $M_{ts}$, 0.90.
(e) Tunnel Mach number, $M_{ts}$, 0.92.
(f) Tunnel Mach number, $M_{ts}$, 0.95.

Figure 27.—Effect of plenum evacuation system flow on pressure coefficient distribution for 3-percent blockage model. Model nose at $x_{ts}/L_{ts} = 0.50$; reentry flaps at 0°; circumferential location of static pressure taps on model, $\varphi$, 0°.

interference-free results on the aft part of the blockage model. The optimum PES flow at each axial location $x/L_R$ for the 3- and 6-percent blockage models (fig. 26) was determined in the following manner. For each $x/L_R$ experimentally determined pressure coefficients were plotted as a function of their associated PES-flow-to-tunnel-flow ratio. The intersection of the curve through these data points with the interference-free pressure coefficient determined the optimum PES flow at a given location. The procedure was then repeated until the optimum PES flow at each of the four $x/L_R$ was determined.

As shown in figure 26 the optimum PES flow tended to increase with increasing tunnel Mach number for both blockage models, but the rate of increase was greater for the 6-percent model. Also, the optimum value of PES flow was greater for the 6-percent blockage model over the entire range of tunnel Mach number investigated. For the 3-percent blockage model the optimum PES flow was essentially constant at 1.4 percent of the tunnel flow as $M_{ts}$ increased from 0.70 to 0.80. Then PES flow increased almost linearly from 1.4 to 2.25 percent of the tunnel flow as $M_{ts}$ increased from 0.80 to 0.95. For the 6-percent blockage model, however, the optimum PES flow increased almost linearly from 1.9 to 3.8 percent of the tunnel flow as $M_{ts}$ increased from 0.70 to 0.95.

### Effect of Reentry Flap Angle

The reentry flaps, as already mentioned, served the same purpose as the PES, which was to provide boundary-layer and model blockage control in the test section. The reentry flaps would not require power, whereas the PES would.

For all the results discussed so far the tunnel reentry flaps were positioned at 9° (figs. 6 and 7). The pressure coefficient axial distribution with the reentry flaps at 0° (i.e., reentry flaps completely closed (figs. 6, 8, and 9)) was similar to that with the reentry flaps at 9°, as shown in figure 27. As expected,

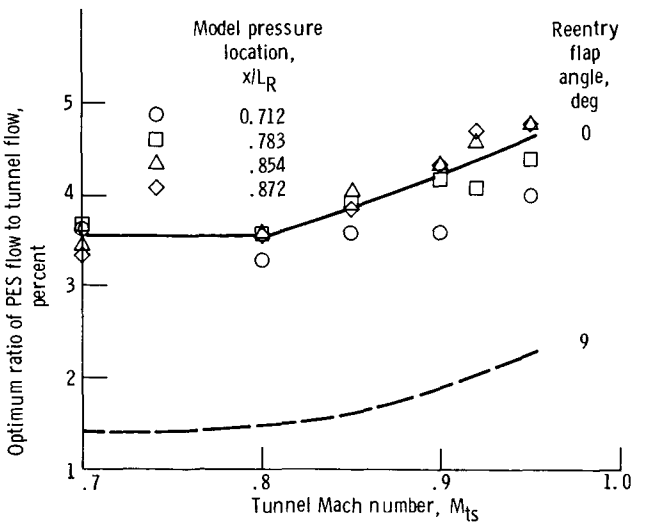


Figure 28.—Effect of reentry flap angle on optimum plenum evacuation system flow for 3-percent blockage model. Model nose at $x_{ts}/L_{ts} = 0.50$.

the level of the pressure coefficient axial distribution on the part of the model not influenced by PES flow (i.e., the forward part of the model surface) was unaffected by reentry flap angle over the entire range of tunnel Mach numbers investigated. Also, as expected, interference-free results were achieved on the aft part of the model with the optimum PES-flow-to-tunnel-flow ratio.

With the reentry flaps at either 0° or 9° (fig. 28) the optimum amount of PES flow increased with increasing tunnel Mach number. However, a much greater amount of PES flow was required when the reentry flaps were at 0° instead of at 9°. For example, at $M_{ts} = 0.95$ the optimum PES flow was reduced from 4.65 to 2.25 percent of tunnel flow when the reentry flap angle was increased from 0° to 9°. This difference in PES flows represents the amount of flow pumped from the plenum chamber into the diffuser by the reentry flaps at their 9° position. This amount of flow, which was substantial, increased only slightly with increasing tunnel Mach numbers—from 2.2 to 2.4 percent of the tunnel flow as $M_{ts}$ increased from 0.70 to 0.95. Thus using tunnel reentry flaps was an effective technique for substantially reducing the amount of flow that must be removed from the plenum chamber by the plenum evacuation system.

## Concluding Remarks

Interference-free results over a range of tunnel Mach numbers from 0.70 to 0.95 should be achievable with the 3- and 6- percent blockage models and possibly also with the 12-percent blockage model installed in a sufficiently long slotted wind tunnel equipped with a plenum chamber and plenum evacuation system (PES) flow capability. With no PES flow the tunnel walls influenced the surface pressure axial distribution on these models. By selecting the proper ratio of PES flow to tunnel flow, however, interference-free results were achieved on the aft part of the 3- and 6-percent blockage models. Therefore interference-free results probably could also be achieved on the aft part of the 12-percent blockage model if it were installed in a sufficiently long slotted test section. No adjustment to the geometry of the eight longitudinal slots was required in this region of the 3- and 6-percent blockage models, and probably none would be required in this region of the 12-percent blockage model.

Achieving interference-free results on the forward part of these models, where PES flow had no influence, however, would be complicated but still possible. It would require varying the width and length of the eight longitudinal slots in the region where the forward part of the models were located. The variation in slot width would be a function of both model blockage ratio and tunnel Mach number; variation in slot length would be a function only of tunnel Mach number. For example, slot width probably would be constant in the region of the forward part of the 3-percent blockage model but would definitely vary in the region of the forward part

of the 6- and 12-percent blockage models. Maximum slot width would decrease with increasing model blockage ratio and increasing tunnel Mach number. Slot length would increase with increasing tunnel Mach number. Thus by varying the slot width and length along with changes in the PES-flow-to-tunnel-flow ratio, the influence of the tunnel walls on the surface pressure of models up to 12-percent blockage probably could be eliminated at tunnel Mach numbers from 0.70 to 0.95.

Although varying the width of the eight longitudinal slots in the region where the forward parts of the models were located is possible, it might not be desirable. An alternative approach would be to narrow these slots (i.e., reduce the test-section open area) enough so that the surface pressures on the forward part of the models would be less than interference-free results. Then PES flow could be used to achieve interference-free results on the forward part as well as on the aft part of the blockage models. The proper amount of PES flow would be a function of axial distance along the forward part of the models. Thus a compartmentalized plenum chamber would be required.

## Summary of Results

An experimental investigation was conducted in the slotted test section of the 0.1-scale model of the proposed Altitude Wind Tunnel. The slotted test section, which had an 11-percent open area ratio, was surrounded by a plenum chamber. The objective was to evaluate wall interference effects at tunnel Mach numbers from 0.70 to 0.95 on bodies of revolution with blockage ratios of 0.43, 3, 6, and 12 percent. The amount of flow required to be removed from the plenum chamber by a plenum evacuation system (PES) to eliminate wall interference effects was determined. The effectiveness of tunnel reentry flaps in removing flow from the plenum chamber was examined with the 3-percent blockage model installed. The results can be summarized as follows:

1. The pressure coefficient axial distribution on the 0.43-percent blockage model was the only one free of wall interference effects with no PES flow.

2. The pressure coefficient axial distribution on the forward part of the 3-, 6-, and 12-percent blockage models was greater than interference-free results and was not influenced by PES flow. The larger the blockage model, the greater the values of the pressure coefficients.

3. Interference-free results were achieved on the aft part of the 3- and 6-percent blockage models with the proper PES-to-tunnel-flow ratio. The value of this ratio increased with increasing tunnel Mach number and increasing blockage model. At a tunnel Mach number of 0.95, PES flows of 2.25 and 3.8 percent of the tunnel flow were required for the 3- and 6-percent blockage models, respectively.

4. It was not possible to determine a value of PES flow to achieve interference-free results on the aft part of the 12-percent blockage model because PES flow influenced only the very small length of the model that was inside the test section.

5. The use of tunnel reentry flaps was an effective technique for substantially reducing the amount of flow required to be removed from the plenum chamber by the PES in order to achieve interference-free results. With the 3-percent blockage model installed and at a tunnel Mach number of 0.95 the PES flow was reduced from 4.65 to 2.25 percent of the tunnel flow when the angle of the reentry flaps was increased from 0° (closed) to 9°.

Lewis Research Center
National Aeronautics and Space Administration
Cleveland, Ohio, January 6, 1987

# Appendix—Method for Setting Tunnel Mach Number

Tunnel Mach number was obtained from a calibration curve that correlated the calculated value of tunnel Mach number with the calculated value of a pressure ratio. The calibration was done in the empty test section. The calibration curve is shown in figure 29. The calculated value of tunnel Mach number was based on measured values of test-section wall static pressure $p_w$ at an axial location $x_{ts}/L_{ts} = 0.18$ and on total pressure at the contraction-section entrance $P_{cs}$. The calculated value of the pressure ratio was based on measured values of plenum-chamber static pressure $p_{pl}$ and total pressure at the contraction-section entrance $P_{cs}$. Note that $P_{cs}$ occurred in the denominator of both the $x$- and $y$-axis parameters. Thus it is only a correlating parameter, and its absolute value is not important for determining tunnel Mach number. What is important, however, is that test-section wall static pressures rather than test-section centerline static pressures were used to calculate tunnel Mach number. (Time limitations precluded using a long slender pipe to measure centerline static pressures.) Consequently using tunnel Mach number as the centerline value required assuming that the centerline static pressures were the same as the wall static pressures. Unpublished results from probes that traversed the test-section radius at three circumferential locations suggested that this was a reasonable assumption. Thus the centerline tunnel Mach number was determined by setting a value of the ratio of plenum-chamber static pressure to contraction-section-entrance total pressure.

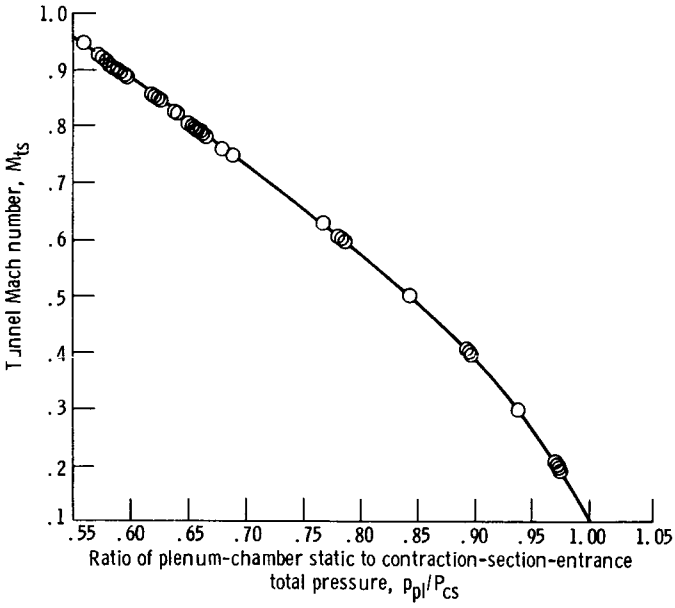


Figure 29.—Calibration curve for obtaining tunnel Mach number.

# References


1. Miller, B.A.; and Chamberlin, R.: Altitude Wind Tunnel (AWT)—A Unique Facility for Propulsion System and Adverse Weather Testing. AIAA Paper 85-0314, Jan. 1985.
2. Blaha, B.J.; and Shaw, R.J.: The NASA Altitude Wind Tunnel: Its Role in Advanced Icing Research and Development. AIAA Paper 85-0090, Jan. 1985.
3. Abbott, J.M., et al.: Analytical and Physical Modeling Program for the NASA Lewis Research Center's Altitude Wind Tunnel (AWT). AIAA Paper 85-0379, Jan. 1985.
4. Towne, C.E., et al.: Analytical Modeling of Circuit Aerodynamics in the New NASA Lewis Altitude Wind Tunnel. AIAA Paper 85-0380, Jan. 1985.
5. Corsiglia, V.R.; Olson, L.E.; and Falarski, M.D.: Aerodynamic Characteristics of the New 40- by 80-/80- by 120-Foot Wind Tunnel at NASA Ames Research Center. AIAA Paper 84-0601, Mar. 1984.
6. van Ditshuizen, J.C.A.: Design and Calibration of the 1/10th Scale Model of the NLR Low Speed Wind Tunnel LST 8×6. Wind Tunnel Design and Testing Techniques, AGARD CP-174, AGARD, 1975, pp. 8-1 to 8-15.
7. Ciepluch, C.C., et al.: Progress in the Lewis Research Center Altitude Wind Tunnel (AWT) Modeling Program. 14th Aerodynamic Testing Conference, AIAA, 1986, pp. 183-192.
8. Gelder, T.F., et al.: Wind Tunnel Turning Vanes of Modern Design. AIAA Paper 86-0044, Jan. 1986.
9. Moore, R.D.; Boldman, D.R.; and Shyne, R.J.: Experimental Evaluation of Two Turning Vane Designs for High Speed Corner of 0.1-Scale Model of NASA Lewis Research Center's Proposed Altitude Wind Tunnel. NASA TP-2570, 1986.
10. Boldman, D.R.; Moore, R.D.; and Shyne, R.J.: Experimental Evaluation of Two Turning Vane Designs for Fan Drive Corner of 0.1-Scale Model of NASA Lewis Research Center's Proposed Altitude Wind Tunnel. NASA TP-2646, 1987.
11. Harrington, D.E.; Burley, R.R.; and Corban, R.R.: Experimental Evaluation of the Wall Mach-Number Distributions of the Octagonal Test Section Proposed for the NASA Lewis Research Center's Altitude Wind Tunnel (AWT). NASA TP-2666, 1986.
12. Burley, R.R.; and Harrington, D.E.: Experimental Evaluation of Honeycomb/Screen Configurations and Short Contraction Section for NASA Lewis Research Center's Proposed Altitude Wind Tunnel. NASA TP-2692, 1987.
13. Couch, L.M.; and Brooks, C.W., Jr.: Effect of Blockage Ratio on Drag and Pressure Distribution for Bodies of Revolution at Transonic Speeds. NASA TN D-7331, 1973.
14. Cahn, M.S.: An Experimental Investigation of Sting-Support Effects on Drag and a Comparison with Jet Effects at Transonic Speeds. NACA Report 1353, 1958.
15. Goethert, B.H.; and Nelson, W.C.: Transonic Wind Tunnel Testing. Pergamon Press, 1961.

| 1. Report No. | 2. Government Accession No. | 3. Recipient's Catalog No. |
|---|---|---|
| NASA TP-2702 | | |

| 4. Title and Subtitle | 5. Report Date |
|---|---|
| Experimental Evaluation of Blockage Ratio and Plenum Evacuation System Flow Effects on Pressure Distribution for Bodies of Revolution in 0.1-Scale Model Test Section of NASA Lewis Research Center's Proposed Altitude Wind Tunnel | April 1987 |
| | 6. Performing Organization Code<br>505-62-3A |
| 7. Author(s)<br>Richard R. Burley and Douglas E. Harrington | 8. Performing Organization Report No.<br>E-3267 |
| | 10. Work Unit No. |
| 9. Performing Organization Name and Address<br>National Aeronautics and Space Administration<br>Lewis Research Center<br>Cleveland, Ohio 44135 | 11. Contract or Grant No. |
| | 13. Type of Report and Period Covered<br>Technical Paper |
| 12. Sponsoring Agency Name and Address<br>National Aeronautics and Space Administration<br>Washington, D.C. 20546 | 14. Sponsoring Agency Code |

15. Supplementary Notes

16. Abstract

An experimental investigation was conducted in the slotted test section of the 0.1-scale model of the proposed Altitude Wind Tunnel to evaluate wall interference effects at tunnel Mach numbers from 0.70 to 0.95 on bodies of revolution with blockage ratios of 0.43, 3, 6, and 12 percent. The amount of flow that had to be removed from the plenum chamber (which surrounded the slotted test section) by the plenum evacuation system (PES) to eliminate wall interference effects was determined. The effectiveness of tunnel reentry flaps in removing flow from the plenum chamber was examined. The 0.43-percent blockage model was the only one free of wall interference effects with no PES flow. Surface pressures on the forward part of the other models were greater than interference-free results and were not influenced by PES flow. Interference-free results were achieved on the aft part of the 3- and 6-percent blockage models with the proper amount of PES flow. The required PES flow was substantially reduced by opening the reentry flaps.

| 17. Key Words (Suggested by Author(s)) | 18. Distribution Statement |
|---|---|
| High subsonic wall interference<br>Blockage ratio<br>Facilities<br>Test-section venting | Unclassified – unlimited<br>STAR Category 09 |

| 19. Security Classif. (of this report) | 20. Security Classif. (of this page) | 21. No of pages | 22. Price* |
|---|---|---|---|
| Unclassified | Unclassified | 25 | A02 |

*For sale by the National Technical Information Service, Springfield, Virginia 22161

NASA-Langley, 1987